A neural circuit mechanism for mechanosensory feedback control of ingestion

https://doi.org/10.1038/s41586-020-2167-2

Received: 11 April 2019

Accepted: 7 February 2020

Published online: 8 April 2020

Check for updates

Dong-Yoon Kim[1,2,6], Gyuryang Heo[1,6], Minyoo Kim[1,3,6], Hyunseo Kim[1], Ju Ae Jin[1], Hyun-Kyung Kim[1,3], Sieun Jung[1,2], Myungmo An[1,3], Benjamin H. Ahn[1,3], Jong Hwi Park[1], Han-Eol Park[1], Myungsun Lee[1,3], Jung Weon Lee[4], Gary J. Schwartz[5] & Sung-Yon Kim[1,2,3]✉

Mechanosensory feedback from the digestive tract to the brain is critical for limiting excessive food and water intake, but the underlying gut–brain communication pathways and mechanisms remain poorly understood[1–12]. Here we show that, in mice, neurons in the parabrachial nucleus that express the prodynorphin gene (hereafter, PB^{Pdyn} neurons) monitor the intake of both fluids and solids, using mechanosensory signals that arise from the upper digestive tract. Most individual PB^{Pdyn} neurons are activated by ingestion as well as the stimulation of the mouth and stomach, which indicates the representation of integrated sensory signals across distinct parts of the digestive tract. PB^{Pdyn} neurons are anatomically connected to the digestive periphery via cranial and spinal pathways; we show that, among these pathways, the vagus nerve conveys stomach-distension signals to PB^{Pdyn} neurons. Upon receipt of these signals, these neurons produce aversive and sustained appetite-suppressing signals, which discourages the initiation of feeding and drinking (fully recapitulating the symptoms of gastric distension) in part via signalling to the paraventricular hypothalamus. By contrast, inhibiting the same population of PB^{Pdyn} neurons induces overconsumption only if a drive for ingestion exists, which confirms that these neurons mediate negative feedback signalling. Our findings reveal a neural mechanism that underlies the mechanosensory monitoring of ingestion and negative feedback control of intake behaviours upon distension of the digestive tract.

Classic experiments have shown that gastric distension suppresses both feeding and drinking, that it is avoided and that its signalling involves vagal and spinal afferents[1–10]. However, the specific circuit mechanism by which mechanosensory feedback signalling from the digestive tract reduces appetite remains largely unclear. The digestive tract is extensively innervated by cranial and spinal afferents that transmit sensory information to the hindbrain nucleus of the solitary tract (NTS)[1–5,13,14]. The NTS—with spinal collaterals—projects to the parabrachial nucleus, which then broadly innervates many forebrain and midbrain areas that are implicated in feeding and drinking[13–15]. This architecture makes the parabrachial nucleus well-suited to have a key role in mechanosensory monitoring and feedback control of ingestion. Indeed, the parabrachial nucleus has previously been functionally implicated in intake behaviours through lesions, pharmacological interventions, cell-type-specific activity manipulations and recordings[15–17]. Therefore, we focused on the parabrachial nucleus to uncover a subpopulation of neurons that encodes mechanosensory signals that arise from the digestive tract upon ingestion and transmits appetite-suppressing signals.

PB^{Pdyn} neurons monitor ingestion

On the basis of FOS immunohistochemistry data showing that PB^{Pdyn} neurons are activated upon water intake, and in situ hybridization experiments showing that these neurons are distinct from *Oxtr*$^{+}$ neurons[16] and *Calca*$^{+}$ neurons[15,18] (Extended Data Fig. 1), we assessed the real-time activity of PB^{Pdyn} neurons using fibre photometry (Fig. 1a, Extended Data Fig. 2a). Notably, PB^{Pdyn} neurons were acutely activated upon water intake, and their activity rapidly returned to the basal level when mice stopped drinking (Fig. 1b, c, Extended Data Fig. 2b, c). PB^{Pdyn} neurons were also activated by the consumption of diverse fluids (liquid food, basic bicarbonate solution, hypertonic saline and silicone oil) as well as solids (hydrogel and chow food) (Fig. 1c–e). Across the intake of distinct fluids and solids, the response amplitude positively correlated with the ingestion rate (Fig. 1f, Extended Data Fig. 3c, d). The activation by the intake of either fluids or solids, and the fact that the response strength scales with the ingestion rate, suggest that PB^{Pdyn} neurons monitor ingestion using mechanosensory signals from the digestive tract.

[1]Institute of Molecular Biology and Genetics, Seoul National University, Seoul, South Korea. [2]Program in Neuroscience, Seoul National University, Seoul, South Korea. [3]Department of Chemistry, Seoul National University, Seoul, South Korea. [4]Department of Pharmacy, Seoul National University, Seoul, South Korea. [5]Department of Medicine and Neuroscience, Albert Einstein College of Medicine, New York, NY, USA. [6]These authors contributed equally: Dong-Yoon Kim, Gyuryang Heo, Minyoo Kim. ✉e-mail: sungyonkim@snu.ac.kr

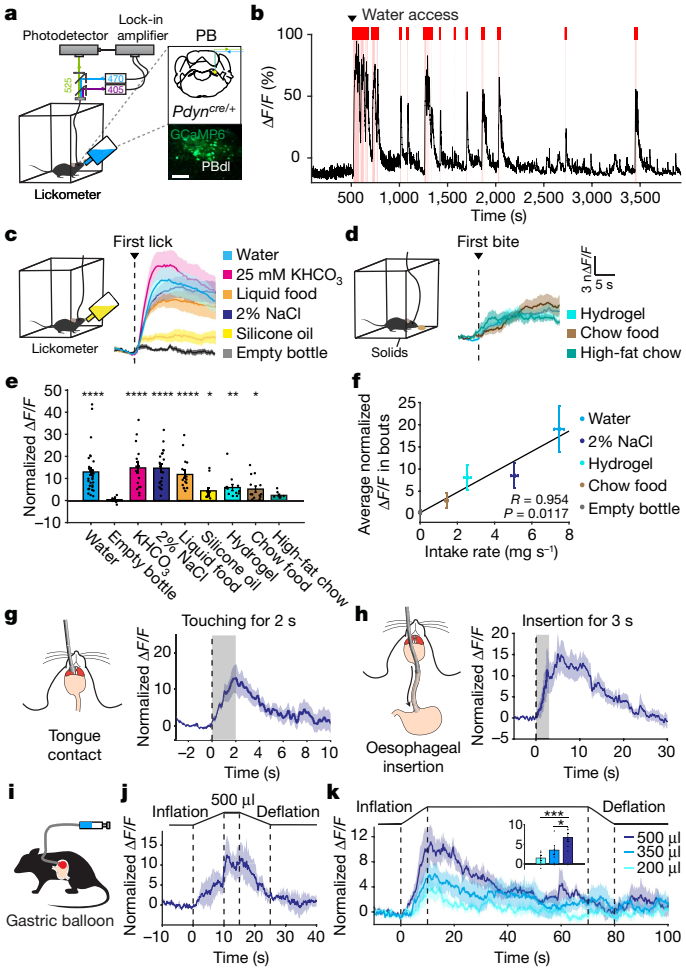

Fig. 1 | PB^{Pdyn} neurons monitor ingestion using mechanosensory signals from the upper digestive tract. a, Fibre photometry recording from PB^{Pdyn} neurons. **b**, Example recording of PB^{Pdyn} neurons during water intake. Red lines, licks; red shaded boxes, bouts. **c**, **d**, Responses of PB^{Pdyn} neurons to the intake of various test liquids (**c**) and solids (**d**). **e**, Average calcium responses during intake bouts. Comparisons against empty-bottle licking are indicated. **f**, Correlation between the intake rate and PB^{Pdyn} neuron activity. **g**, **h**, PB^{Pdyn} neurons were robustly activated by touching the tongue (**g**) or inserting gavage needle through the oesophagus (**h**). **i**–**k**, Gastric balloon inflation for mechanical distension of the stomach (**i**). **j**, PB^{Pdyn} neurons showed an increase and decrease in activity during balloon inflation and deflation, respectively, without prolonged responses. **k**, The response amplitude scaled with the inflated volume, and prolonged maintenance of balloon inflation revealed adaptation-like changes. Inset, average calcium responses in the first 30 s of inflation. Scale bar, 100 µm. Data are mean ± s.e.m. $^{*}P < 0.05$, $^{**}P < 0.01$, $^{***}P < 0.001$, $^{****}P < 0.0001$. For statistics, see Supplementary Table 1.

Signalling of digestive tract distension

To directly test this possibility, we applied diverse mechanical stimuli to different parts of the digestive tract. First, touching the tongue with a gavage needle evoked robust responses in PB^{Pdyn} neurons (Fig. 1g). Inserting the gavage needle into the oesophagus (which touches and stretches the oesophageal wall) also robustly activated PB^{Pdyn} neurons (Fig. 1h). Furthermore, PB^{Pdyn} neurons strongly responded to the inflation of an intragastric balloon in an inflation-rate-dependent manner (Fig. 1i–k). Notably, maintaining balloon inflation for an extended duration revealed adaptation-like responses, reminiscent of the responses of mechanosensory neurons in the parabrachial nucleus and vagal afferents to gastric distension[19,20]. Locally pushing the stomach wall, and directly injecting liquids or air into each part of the upper digestive tract using oral gavage or a gastric catheter, also strongly activated PB^{Pdyn} neurons (Extended Data Figs. 2d–l, 3a, b). By contrast, PB^{Pdyn} neurons did not significantly respond to the balloon-mediated distension of either the duodenum or proximal colon (Extended Data Figs. 2m, n, 3e, f). Thus, the activity of PB^{Pdyn} neurons encodes mechanosensation from the upper parts of the digestive tract.

In a series of control experiments, we observed that the responses of PB^{Pdyn} neurons are not modulated by the taste, osmolality or temperature of ingesta (Extended Data Fig. 2o–r). We also found that the activity of the PB^{Pdyn} neuron population was not related to general locomotion or anxiety, and that these neurons were unresponsive to dorsum stroke, whisker touch, sensory detection of peanut butter or a conditioned tone that predicted water delivery (Extended Data Fig. 4a–h). Moreover, neither the baseline activity nor the responses of PB^{Pdyn} neurons were modulated by the internal need state (Extended Data Fig. 5). Collectively, our findings suggest that a major role of PB^{Pdyn} neurons is signalling interoceptive mechanosensation from the upper digestive tract for monitoring ingestion.

Representation of integrated signals

Given that the PB^{Pdyn} neuron population is activated by stimuli that are seemingly distinct (ranging from water and food intake to mechanical stimulation of parts of the digestive tract), we investigated how these stimuli are represented by individual PB^{Pdyn} neurons using two-photon microscopy (Fig. 2a, b). We first examined the representation of ingestion. Consistent with our FOS experiments, the intake of water and liquid food acutely and robustly activated about 82% and about 75% of PB^{Pdyn} neurons, respectively (Fig. 2c–e). Notably, the registration of neurons across trials revealed that these two populations were mostly overlapping (Fig. 2f), and their response amplitudes exhibited a linear correlation (Fig. 2g). Thus, the majority of PB^{Pdyn} neurons respond to the ingestion of both water and liquid food.

We next examined the representation of gastric distension (Fig. 2h). Consistent with the results from fibre photometry recordings (Fig. 1i–k), we observed robust activation in most PB^{Pdyn} neurons (Fig. 2i, j). Increasing the inflation volume tended to increase both the response strength (Fig. 2k, l) and the number of activated neurons (Fig. 2m). We also monitored the responses of PB^{Pdyn} neurons to oral delivery of a liquid drop (10 µl) (Fig. 2n). This also evoked robust responses in a large fraction of PB^{Pdyn} neurons (76.3%) (Fig. 2o, p). The registration of neurons across experiments revealed that most PB^{Pdyn} neurons responded to water intake, gastric distension and oral delivery of a liquid drop (Fig. 2q), which comprise stimuli transmitted through different cranial and spinal nerve pathways[1–5,13,14]. Thus, the majority of PB^{Pdyn} neurons represent integrated visceral mechanosensory signals from distinct organs of the digestive tract. Furthermore, because the same neurons are activated by ingestion and by distension of the digestive tract, these results strongly support the notion that PB^{Pdyn} neurons monitor ingestion using integrated mechanosensory signals from the digestive tract.

Vagus nerve signals gastric distension

We next considered how the PB^{Pdyn} neuron population receives mechanosensory signals from the digestive tract. To answer this question, we first mapped the monosynaptic inputs of PB^{Pdyn} neurons using engineered rabies viruses (Fig. 3a, Methods). The monosynaptic input neurons were found throughout the brain (Fig. 3b, Extended Data Fig. 6a), but notably in the trigeminal nerve nuclei and specific subregions of the NTS that receive oral, oropharyngeal and visceral sensory information transmitted via the trigeminal, facial, glossopharyngeal and vagus nerves[13] (Fig. 3c). Additional synaptic spread of the virus from the primary sensory trigeminal nucleus or NTS revealed input neurons in the cranial nerve ganglia (Fig. 3d, e, Extended Data Fig. 6b–e), confirming the anatomical connectivity between PB^{Pdyn} neurons and cranial afferent pathways.

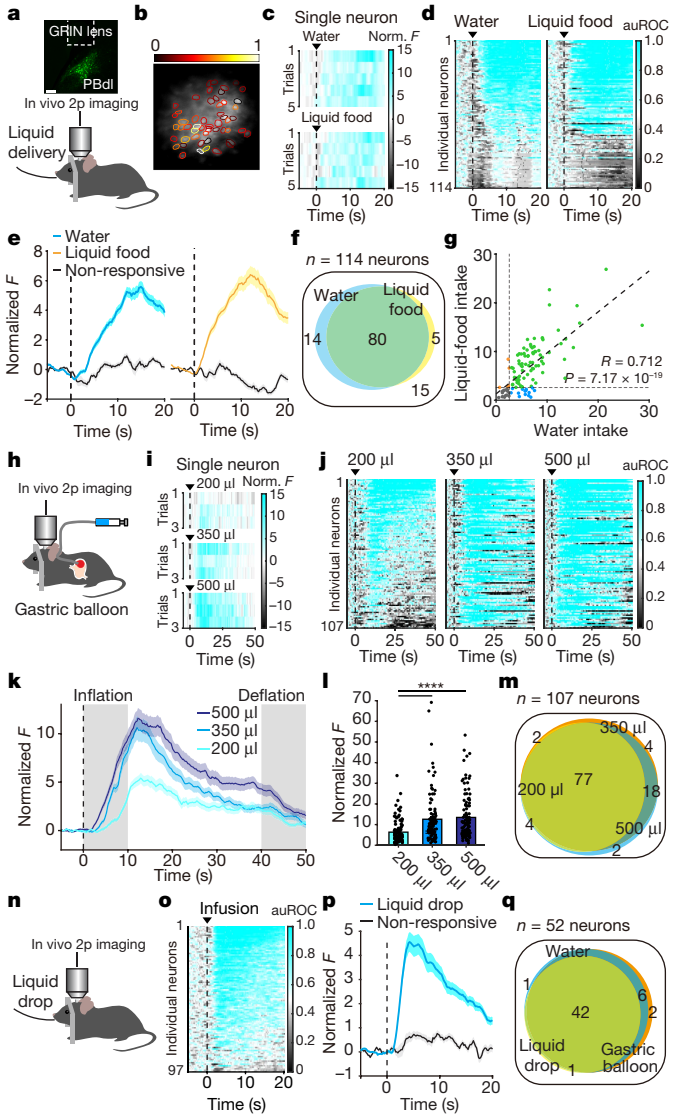

Fig. 2 | Representation of integrated mechanosensory signals by individual PB^{Pdyn} neurons. a, Two-photon calcium imaging of PB^{Pdyn} neurons during oral delivery of water or liquid food. **b**, Representative two-photon image of PB^{Pdyn} neurons. Colours indicate the normalized calcium responses in the first 20 s of water infusion. **c**, Responses of an example neuron. Norm., normalized. **d**, Responses of all neurons averaged across all trials. auROC, area under the receiver operating characteristic. **e**, Average calcium traces from significantly activated or non-responsive neurons. **f**, Distribution and overlap of responsive neurons. **g**, Correlation between the response amplitudes for the intake of water or liquid food. **h**, Two-photon imaging of PB^{Pdyn} neurons during intragastric balloon inflation (10-s inflation, 30-s maintenance and 10-s deflation). **i**, Responses of an example neuron. **j**, Trial-averaged responses of all neurons. **k**, Average calcium traces from significantly activated PB^{Pdyn} neurons. **l**, Average activity in the first 30 s of intragastric balloon inflation. **m**, Distribution and overlap of responsive neurons. **n**, Two-photon imaging of PB^{Pdyn} neurons during oral delivery of small liquid drop (water and liquid food pooled). **o**, Trial-averaged responses of all neurons. **p**, Average calcium traces from significantly activated or non-responsive neurons. **q**, Distribution and overlap of responsive neurons. Dotted lines indicate the stimulus onset. Scale bar, 150 µm. Data are mean ± s.e.m. ****$P < 0.0001$. For statistics, see Supplementary Table 1.

The commonly held notion is that physiological gastric distension and visceral pain are relayed by vagal and spinal pathways, respectively[14,21], but several studies have implicated a role for spinal afferents in the mechanosensory feedback signalling of ingestion[2,21]. Indeed, we also found that some neurons in the dorsal horn provide direct inputs to

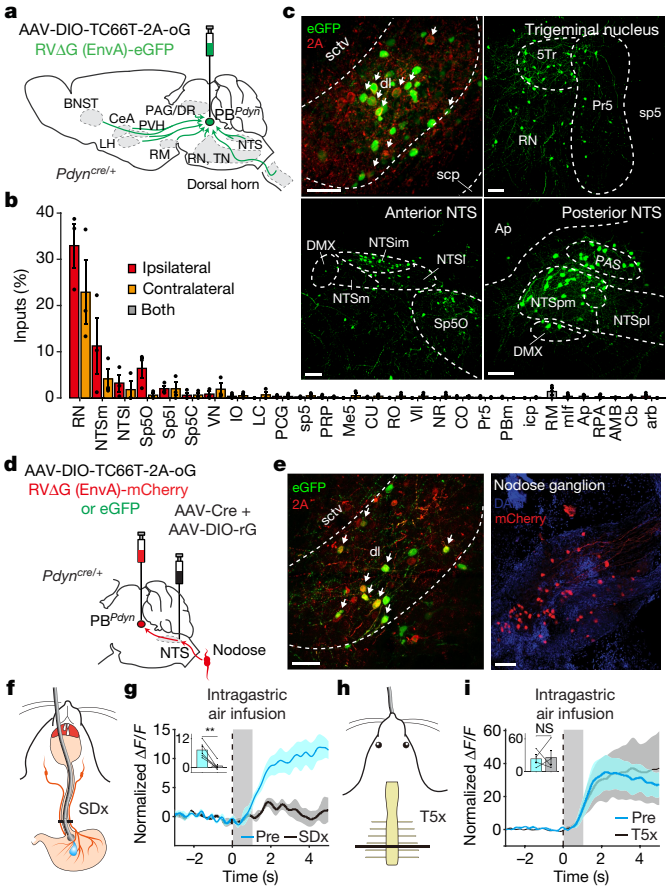

Fig. 3 | The vagus nerve conveys gastric distension signals to PB^{Pdyn} neurons. a, Engineered rabies-virus-mediated identification of monosynaptic inputs to PB^{Pdyn} neurons. **b**, Quantification of monosynaptic inputs in the hindbrain, shown as the per cent of labelled neurons from a given brain region relative to the total labelled neurons throughout the hindbrain. **c**, Confocal images showing the injection site (starter cells indicated with arrows) and labelled neurons in select upstream regions in the hindbrain. **d**, Engineered rabies-virus-mediated identification of monosynaptic inputs to the NTS neurons that project to PB^{Pdyn} neurons. **e**, Representative images showing starter cells (left, arrows) and labelled neurons in the nodose ganglion projecting to the NTS neurons that project to PB^{Pdyn} neurons (right). **f**–**i**, Total subdiaphragmatic vagotomy (SDx) (**f**) abolished the response of PB^{Pdyn} neurons to intragastric air injection (**g**), but thoracic level-5 spinal transection (T5x) (**h**) did not (**i**). Insets show average responses in the first 5 s of injection. Scale bars, 100 µm. Data are mean ± s.e.m. **$P < 0.01$; NS, not significant. For statistics, see Supplementary Table 1. Definitions for the abbreviations are given in 'Abbreviations' in Methods.

PB^{Pdyn} neurons (Extended Data Fig. 6a). To determine the pathway that conveys mechanosensory signals to PB^{Pdyn} neurons, we tested whether vagotomy or spinal transection abolishes the responses of PB^{Pdyn} neurons to gastric distension. Notably, the responses were fully abolished by subdiaphragmatic vagotomy, but not after spinal transection (Fig. 3f–i, Extended Data Fig. 6f–k). Thus, mechanosensory signals from the stomach reach PB^{Pdyn} neurons via vagal—not spinal—pathways. We further found that PB^{Pdyn} neurons are activated by the systemic injection of cholecystokinin (CCK), a gut hormone that has previously been shown to stimulate vagal afferents that are sensitive to gastric distension[19,22], which corroborates the idea that PB^{Pdyn} neurons receive gastric distension signals via mechanosensory vagal fibres (Extended Data Fig. 6l).

PB^{Pdyn} neurons suppress ingestion

We next sought to determine the causal function of PB^{Pdyn} neurons using chemogenetic and optogenetic tools. Notably, chemogenetic

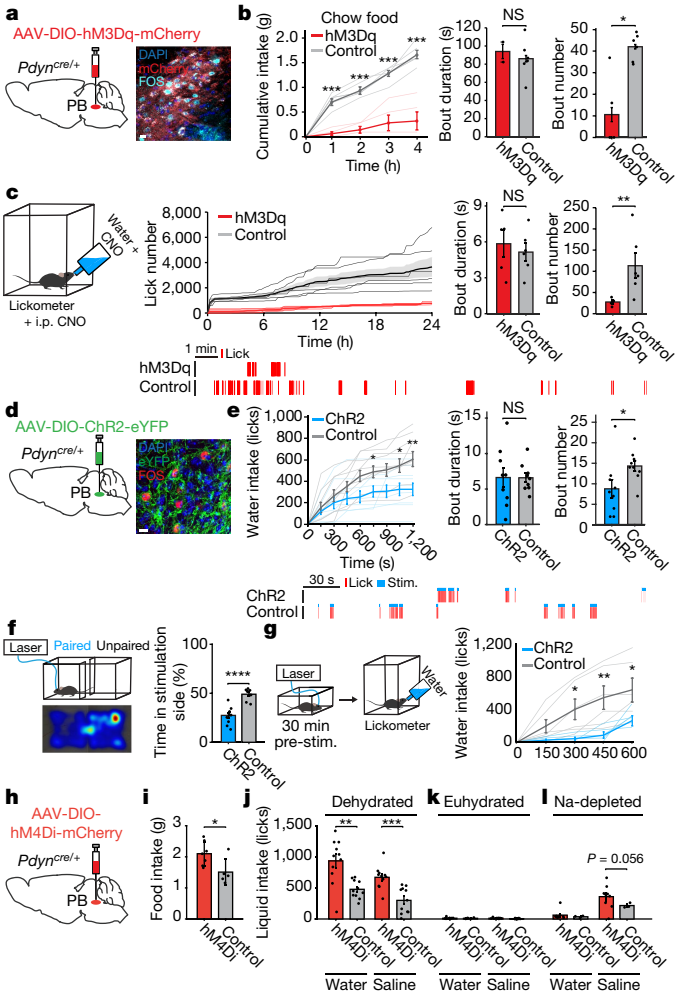

Fig. 4 | PB^{Pdyn} neurons transmit sustained appetite-suppressing signals to discourage the initiation of ingestion. a–**c**, Chemogenetic stimulation of PB^{Pdyn} neurons (**a**) suppressed food intake in food-deprived mice by decreasing bout number, not duration (**b**). This manipulation also inhibited water intake by decreasing bout number (**c**). Bottom, representative example traces. Confocal image shows high overlap between hM3Dq-expressing and clozapine *N*-oxide (CNO)-injection-induced FOS-expressing neurons. i.p., intraperitoneal. **d**, **e**, Lick-paired optogenetic stimulation of PB^{Pdyn} neurons (**d**) also did not affect bout duration, but reduced bout number to inhibit water intake (**e**). Bottom, representative example traces. Representative confocal image (**d**) shows high overlap between ChR2-expressing and photostimulation-induced FOS-expressing neurons. **f**, Optogenetic stimulation of PB^{Pdyn} neurons was avoided in a real-time place preference test. **g**, Pre-stimulation of PB^{Pdyn} neurons for 30 min before the session produced sustained inhibition of drinking in dehydrated mice. **h**–**l**, Chemogenetic inhibition of PB^{Pdyn} neurons (**h**) increased the intake of chow food in fasted mice (**i**), and both water and hypertonic saline in dehydrated (**j**), but not in euhydrated (**k**), mice. This manipulation tended to increase the intake of hypertonic saline in salt-depleted mice (**l**). Scale bars, 10 µm. Data are presented as mean ± s.e.m. $^*P < 0.05$, $^{**}P < 0.01$, $^{***}P < 0.001$, $^{****}P < 0.0001$, NS, not significant. For statistics, see Supplementary Table 1.

stimulation of PB^{Pdyn} neurons potently suppressed food and water intake, and these effects were mediated by a reduction in the number of bouts rather than decreases in bout duration (Fig. 4a–c, Extended Data Fig. 7a). Brief optogenetic stimulation of PB^{Pdyn} neurons upon the detection of each lick or stimulation throughout the entire session also suppressed fluid intake by reducing bout number (Fig. 4d, e, Extended Data Fig. 7b–j). Thus, activity in PB^{Pdyn} neurons suppresses ingestion by deterring the initiation of intake bouts, rather than terminating initiated bouts. Importantly, the effect of activating PB^{Pdyn} neurons mimics the symptoms of gastric distension, as gastric distension also suppresses water intake by reducing the number of bouts rather than their duration[9] (Extended Data Fig. 7l–s). This suggests that PB^{Pdyn} neurons may mediate the suppression of appetite that is induced by distension of the digestive tract.

To gain insights into how PB^{Pdyn} neurons suppress ingestion, we further explored their causal functions. As with previous findings that gastric distension is avoided in rats and humans[6,7], we also found that PB^{Pdyn} neurons transmit a negative-valence signal regardless of the internal state of mice (Fig. 4f, Extended Data Fig. 7k). On the other hand, our observations that PB^{Pdyn} neurons are most active at the beginning of intake, and that lick-paired brief stimulations do not reduce bout duration, suggest that PB^{Pdyn} neurons produce sustained appetite-suppressing signals that exert effects over a prolonged time. Indeed, pre-stimulation of PB^{Pdyn} neurons before water-intake assays suppressed drinking for at least 10 min (Fig. 4g). As behavioural controls, we found that activating PB^{Pdyn} neurons did not affect social or anxiety-like behaviours (Extended Data Fig. 4i, j). Together, our data show that the mechanism by which PB^{Pdyn} neurons inhibit ingestive behaviours is through transmitting sustained appetite-suppressing signals, and that the effects of activating PB^{Pdyn} neurons matches well with the symptoms of gastric distension.

Negative feedback control of ingestion

To assess the physiological role of signals transmitted by PB^{Pdyn} neurons, we next chemogenetically inhibited PB^{Pdyn} neurons (Fig. 4h). This manipulation increased the intake of chow food in food-deprived mice (Fig. 4i), and the intake of both water and hypertonic saline in dehydrated mice (Fig. 4j). Notably, inhibiting PB^{Pdyn} neurons did not affect the intake of either water or saline in euhydrated mice (Fig. 4k), and elicited a trend towards an increased intake of hypertonic saline (but not water) in salt-depleted mice (Fig. 4l). Thus, the reduced activity of PB^{Pdyn} neurons causes overconsumption only when the appetite already exists, rather than stimulating appetite by itself—akin to the effects elicited by loss-of-function manipulation of many gut-borne biochemical feedback signals[10]. These results show that PB^{Pdyn} neurons are required for the negative feedback control of ingestion.

To better understand the circuit mechanism by which PB^{Pdyn} neurons control ingestion, we investigated the output circuits. Projection mapping revealed that PB^{Pdyn} neurons densely innervate many brain areas that are critical for intake behaviours (Extended Data Fig. 8a). Among the targets known to have a central role in the regulation of appetite and thirst, optogenetic stimulation of projections to the paraventricular hypothalamus[23–26] potently suppressed intake, and produced negative-valence signals (Extended Data Fig. 8b–g), similar to PB^{Pdyn} soma stimulation and gastric distension. By contrast, stimulating projections to the subfornical organ[11,12] did not affect either feeding or drinking, but did produce negative-valence signals (Extended Data Fig. 8h–k). These results suggest that the paraventricular hypothalamus is a downstream projection target of PB^{Pdyn} neurons that at least partially mediates the suppression of ingestion, probably via its appetite-suppressing subpopulations[24–26].

Discussion

Our findings collectively reveal a mechanism by which mechanosensation from the upper digestive tract is integrated and transduced to a negative sensory feedback signal that reduces appetite; a summary model is provided in Extended Data Fig. 9. The activity of PB^{Pdyn} neurons seems to encode instantaneous changes in the volume of the digestive tract, rather than the steady-state volume; by providing appetite-suppressing feedback signals that scale with the ingestion rate, PB^{Pdyn} neurons may serve to protect the organism against the potential harm associated with overconsumption. This aligns well with

findings that implicate neurons of the parabrachial nucleus in alarm functions[15,27]. Furthermore, our two-photon imaging and tracing data suggest that PB^{Pdyn} neurons represent a convergent circuit node for the integration of mechanosensory information from the upper digestive tract[20]. Where and how mechanosensory signals from distinct organs are transmitted and converged to create an integrated representation are questions that are not yet resolved.

Appetite can be suppressed by satiating thirst or hunger, or by introducing a competing motivational state[4–6,10,15,28]. Because distension of the digestive tract does not fundamentally resolve hunger or thirst (that is, by replenishing nutrients or water), we speculate that PB^{Pdyn} neurons introduce a physiological anorexic state that competes with hunger or thirst (that is distinct from pathological anorexia mediated by neurons in the external lateral parabrachial nucleus[15,18]). This might be mediated by appetite-suppressing neurons in the downstream targets, including *Pdyn*$^+$ (ref. [25]) and *Crh*$^+$ (ref. [26]) neurons of the paraventricular hypothalamus and *Prkcd*$^+$ neurons of the central amygdala[29]. On the other hand, the many monosynaptic inputs to PB^{Pdyn} neurons found throughout the brain indicate the existence of regulation from upstream regions.

Mechanosensory feedback signals would work in concert with other feedback mechanisms that are based on diverse features of ingesta, such as nutrition[10,30,31], osmolality, taste and temperature[11,12]. Distinct feedback mechanisms use neural and hormonal signals that arise from different parts of the digestive tract, which may influence ingestive behaviours in a stepwise fashion[1–12,17,30–33]. Identifying the circuit mechanisms that integrate these inputs, as well as the internal needs, to determine the behavioural output[1–5,11,12], will provide further insights into the principles of ingestive behaviour. In a clinical perspective, our findings shed light on the mechanisms that underlie gastric balloon therapy, gastric bypass surgery (in which the distension of the remaining stomach after the operation can be exaggerated upon ingestion) and vagus nerve stimulation for the treatment of obesity and diabetes[34]. The function of specific circuits resolved in this study may represent potential targets for therapeutic strategies that aim to treat obesity and related metabolic disorders.

Online content

Any methods, additional references, Nature Research reporting summaries, source data, extended data, supplementary information, acknowledgements, peer review information; details of author contributions and competing interests; and statements of data and code availability are available at https://doi.org/10.1038/s41586-020-2167-2.

1. Schwartz, G. J. The role of gastrointestinal vagal afferents in the control of food intake: current prospects. *Nutrition* **16**, 866–873 (2000).
2. Cummings, D. E. & Overduin, J. Gastrointestinal regulation of food intake. *J. Clin. Invest.* **117**, 13–23 (2007).
3. Umans, B. D. & Liberles, S. D. Neural sensing of organ volume. *Trends Neurosci.* **41**, 911–924 (2018).
4. Andermann, M. L. & Lowell, B. B. Toward a wiring diagram understanding of appetite control. *Neuron* **95**, 757–778 (2017).
5. Gizowski, C. & Bourque, C. W. The neural basis of homeostatic and anticipatory thirst. *Nat. Rev. Nephrol.* **14**, 11–25 (2018).
6. Miller, N. E. Experiments on motivation. *Science* **126**, 1271–1278 (1957).
7. Salet, G. A. M., Samsom, M., Roelofs, J. M. M., van Berge Henegouwen, G. P., Smout, A. J. P. M. & Akkermans, L. M. A. Responses to gastric distension in functional dyspepsia. *Gut* **42**, 823–829 (1998).
8. Powley, T. L. & Phillips, R. J. Gastric satiation is volumetric, intestinal satiation is nutritive. *Physiol. Behav.* **82**, 69–74 (2004).
9. Eisen, S., Davis, J. D., Rauhofer, E. & Smith, G. P. Gastric negative feedback produced by volume and nutrient during a meal in rats. *Am. J. Physiol. Regul. Integr. Comp. Physiol.* **281**, R1201–R1214 (2001).
10. Berthoud, H.-R. Vagal and hormonal gut–brain communication: from satiation to satisfaction. *Neurogastroenterol. Motil.* **20** (Suppl 1), 64–72 (2008).
11. Zimmerman, C. A., Leib, D. E. & Knight, Z. A. Neural circuits underlying thirst and fluid homeostasis. *Nat. Rev. Neurosci.* **18**, 459–469 (2017).
12. Augustine, V., Lee, S. & Oka, Y. Neural control and modulation of thirst, sodium appetite, and hunger. *Cell* **180**, 25–32 (2020).
13. Contreras, R. J., Beckstead, R. M. & Norgren, R. The central projections of the trigeminal, facial, glossopharyngeal and vagus nerves: an autoradiographic study in the rat. *J. Auton. Nerv. Syst.* **6**, 303–322 (1982).
14. Saper, C. B. The central autonomic nervous system: conscious visceral perception and autonomic pattern generation. *Annu. Rev. Neurosci.* **25**, 433–469 (2002).
15. Palmiter, R. D. The parabrachial nucleus: CGRP neurons function as a general alarm. *Trends Neurosci.* **41**, 280–293 (2018).
16. Ryan, P. J., Ross, S. I., Campos, C. A., Derkach, V. A. & Palmiter, R. D. Oxytocin-receptor-expressing neurons in the parabrachial nucleus regulate fluid intake. *Nat. Neurosci.* **20**, 1722–1733 (2017).
17. McKinley, M. J. & Johnson, A. K. The physiological regulation of thirst and fluid intake. *Physiology* **19**, 1–6 (2004).
18. Carter, M. E., Soden, M. E., Zweifel, L. S. & Palmiter, R. D. Genetic identification of a neural circuit that suppresses appetite. *Nature* **503**, 111–114 (2013).
19. Schwartz, G. J., McHugh, P. R. & Moran, T. H. Integration of vagal afferent responses to gastric loads and cholecystokinin in rats. *Am. J. Physiol. Regul. Integr. Comp. Physiol.* **261**, R64–R69 (1991).
20. Karimnamazi, H., Travers, S. P. & Travers, J. B. Oral and gastric input to the parabrachial nucleus of the rat. *Brain Res.* **957**, 193–206 (2002).
21. Grundy, D. & Scratcherd, T. in *Comprehensive Physiology* (ed. Terjung, R.) https://doi.org/10.1002/cphy.cp060116 (2011).
22. Williams, E. K. et al. Sensory neurons that detect stretch and nutrients in the digestive system. *Cell* **166**, 209–221 (2016).
23. Garfield, A. S. et al. A neural basis for melanocortin-4 receptor-regulated appetite. *Nat. Neurosci.* **18**, 863–871 (2015).
24. Li, C. et al. Defined paraventricular hypothalamic populations exhibit differential responses to food contingent on caloric state. *Cell Metab.* **29**, 681–694.e5 (2019).
25. Li, M. M. et al. The paraventricular hypothalamus regulates satiety and prevents obesity via two genetically distinct circuits. *Neuron* **102**, 653–667.e6 (2019).
26. Kim, J. et al. Rapid, biphasic CRF neuronal responses encode positive and negative valence. *Nat. Neurosci.* **22**, 576–585 (2019).
27. Barik, A., Thompson, J. H., Seltzer, M., Ghitani, N. & Chesler, A. T. A brainstem–spinal circuit controlling nocifensive behavior. *Neuron* **100**, 1491–1503.e3 (2018).
28. Burnett, C. J. et al. Hunger-driven motivational state competition. *Neuron* **92**, 187–201 (2016).
29. Cai, H., Haubensak, W., Anthony, T. E. & Anderson, D. J. Central amygdala PKC-δ$^+$ neurons mediate the influence of multiple anorexigenic signals. *Nat. Neurosci.* **17**, 1240–1248 (2014).
30. Beutler, L. R. et al. Dynamics of gut–brain communication underlying hunger. *Neuron* **96**, 461–475.e5 (2017).
31. Su, Z., Alhadeff, A. L. & Betley, J. N. Nutritive, post-ingestive signals are the primary regulators of AgRP neuron activity. *Cell Rep.* **21**, 2724–2736 (2017).
32. Bai, L. et al. Genetic identification of vagal sensory neurons that control feeding. *Cell* **179**, 1129–1143.e23 (2019).
33. Han, W. et al. A neural circuit for gut-induced reward. *Cell* **175**, 665–678.e23 (2018).
34. de Lartigue, G. Role of the vagus nerve in the development and treatment of diet-induced obesity. *J. Physiol.* **594**, 5791–5815 (2016).

Methods

Mice

All mice were housed in a temperature- and humidity-controlled room with a reverse 12-h light/dark cycle and ad libitum access to chow food and water, unless otherwise noted. Both male and female mice of at least six weeks of age were used for data collection. C57BL/6J (JAX stock no. 000664), *Pdyn*$^{cre/+}$ (JAX stock no. 027958) and *Gt(Rosa)26Sor*$^{tm14(CAG-tdTomato)Hze/J}$ (Ai14) (JAX stock no. 007914) mice were obtained from the Jackson Laboratory. All mice used for experiments were heterozygotes maintained on the C57BL/6J background. For the FOS experiment, *Pdyn*$^{cre/+}$ mice were crossed with Ai14 mice to reveal expression patterns. Mice in each litter were randomly assigned to either experimental or control groups. All behavioural procedures were performed during the dark cycle. Before testing, mice were acclimated to the test room for at least 5 min. To facilitate the observation of neural responses to the ingestion of fluids and foods, mice were food- or water-deprived to induce robust ingestive behaviours. Water-deprived (dehydrated) or food-deprived conditions were induced by housing mice without water or food, respectively, for 48 h, unless otherwise noted. All experimental protocols were approved by the Seoul National University Institutional Animal Care and Use Committee, and all experiments were performed in accordance with the Guide for Care and Use of Laboratory Animals from the Seoul National University.

Viral constructs

The recombinant adeno-associated virus (AAV) vectors expressing GCaMP6m (AAV1-hSyn-FLEX-GCaMP6m, 1.2×10^{13} copies per ml) and tdTomato (AAV1-CAG-FLEX-tdTomato, 3.1×10^{12} copies per ml) were purchased from the Penn Vector Core, and the AAV vectors expressing ChR2 (AAV5-EF1α-DIO-hChR2(H134R)-eYFP, 3.2×10^{12} copies per ml) and enhanced yellow fluorescent protein (eYFP) (AAV5-EF1a-DIO-eYFP, 3.2×10^{12} copies per ml) were obtained from the UNC vector core. The AAV vectors expressing hM3Dq (AAV8-hSyn-DIO-hM3D(Gq)-mCherry, 3.0×10^{12} copies per ml), hM4Di (AAV8-hSyn-DIO-hM4D(Gi)-mCherry, 4.0×10^{12} copies per ml) and mCherry (AAV9-hSyn-DIO-mCherry, 2.1×10^{12} copies per ml) were purchased from Addgene, and the AAV vectors expressing ChR2 (AAV-DJ-EF1a-DIO-hChR2(H134R)-eYFP, 4.7×10^{13} copies per ml), eYFP (AAV-DJ-EF1a-DIO-eYFP, 8.8×10^{12} copies per ml), Cre recombinase (AAV-DJ-CMV-eGFP-Cre or AAV-DJ-EF1a-mCherry-IRES-Cre-WPRE) and mRuby-fused synaptophysin (AAV-DJ-hSyn-FLEX-GFP-2A-Synaptophysin-mRuby, 4.0×10^{13} copies per ml) were purchased from the Stanford Vector Core. The AAV vector expressing optimized rabies G protein[35] and enhanced-expression TVA receptor[36] (AAV8-DIO-TC66T-2A-oG, 1.64×10^{13} copies per ml), blue fluorescent protein (BFP)-fused rabies G protein (AAV1-EF1a-DIO-hBFP-RVG) and the recombinant EnvA-pseudotyped G-deficient rabies virus vector expressing GFP (RV-EnvA-ΔG-GFP) and mCherry (RV-EnvA-ΔG-mCherry) were purchased from the Salk vector core. Some rabies vectors (RV-EnvA-ΔG-GFP) were generously provided by B. K. Lim.

Stereotaxic surgery

Mice were anaesthetized with 1.5–3.0% isoflurane and placed in a stereotaxic apparatus (David Kopf Instruments) while resting on a heating pad. A small craniotomy, following a scalp incision, was made using a hand drill at the regions of interest. Between 100 and 300 nl of viral vectors was injected to the centre of the lateral parabrachial nucleus using a pressure injection system (Nanoliter 2000) using a pulled-glass capillary at 40–100 nl min^{-1}. The coordinates for the parabrachial nucleus were −5.4 mm anteroposterior (AP), ±1.25 mm mediolateral (ML) and −3.5 mm dorsoventral (DV); in some mice, for more reliable targeting (or in the case of bilateral implants), we targeted the same region at −10 degrees (−5.4 mm AP, ±0.6 mm ML and −3.5 mm DV) or 10 degrees (−5.3 mm AP, ±1.8 mm ML and −3.1 DV) angle relative to the sagittal plane. The incision was closed using suture and tissue adhesive (Vetbond) and mice were provided with antibiotics and analgesics. Mice were placed in a clean cage on a heating pad to recover from anaesthesia and were kept in their home cage for 2–4 weeks for viral expression and recovery from surgery before behavioural testing. Except for the midline structures, the choice of left or right hemisphere was counterbalanced for all unilateral injections and implantations.

For fibre photometry experiments, recombinant AAVs expressing GCaMP6m were unilaterally injected into the parabrachial nucleus of *Pdyn*$^{cre/+}$ mice, and a low-autofluorescence 400-μm-core, 0.48-NA fibre optic cannula (Doric Lenses) was implanted 0–100 μm above the virus injection site. The fibre optic cannulas were affixed to the skull with C&B Metabond (Parkell) and dental cement. For the experiments involving head fixation, a custom-made stainless steel bar[37] ($4.0 \times 1.0 \times 1.0$ mm^3) was attached to the dental cement during surgery to allow subsequent head fixation to a custom-made station with complementary slots that can accommodate the tips of the attached bars.

For two-photon imaging experiments, GCaMP6m was expressed as above. A custom-built stainless-steel blunt needle (0.5-mm diameter) was lowered to the target coordination to create enough hollow space for lens implantation. The needle was withdrawn after 30 min, and a microendoscopic lens (gradient refractive index lens, 6.1-mm length and 0.5-mm diameter) (Inscopix 1050-002182) was immediately implanted directly above the dorsal lateral parabrachial nucleus (−5.4 mm AP, ±1.25 mm ML and −3.5 mm DV) at coordinates slightly different to those of the viral injection site (−5.2 mm AP, ±1.25 mm ML and −3.5 mm DV) to avoid imaging autofluorescence usually found at the injection track. A custom-made stainless steel bar[37] ($4.0 \times 1.0 \times 1.0$ mm^3) or a ring[38] (3.5-mm inner diameter, 11-mm outer diameter) was attached to the dental cement during surgery for head fixation.

For cell soma optogenetic stimulation experiments, recombinant AAVs expressing ChR2 or eYFP were bilaterally injected into the parabrachial nucleus of *Pdyn*$^{cre/+}$ mice, and 200-μm-core, 0.22-NA fibre optic cannulas (Newdoon) were bilaterally inserted 100–300 μm above the virus injection site. For some control groups, *Pdyn*$^{+/+}$ littermates were injected with AAVs expressing ChR2.

For chemogenetic stimulation or inhibition experiments, recombinant AAVs expressing hM3Dq, hM4Di or tdTomato, mCherry and eYFP were bilaterally injected into the parabrachial nucleus of *Pdyn*$^{cre/+}$ mice.

For terminal optogenetic stimulation experiments, recombinant AAVs expressing ChR2 or eYFP were bilaterally injected into the parabrachial nucleus of *Pdyn*$^{cre/+}$ mice, and 200-μm-core fibre optic cannulas were implanted above the subfornical organ (−0.6 mm AP, 0 mm ML and −2.6 mm DV) or paraventricular hypothalamus (−0.6 mm AP, 0 mm ML and −4.2 mm DV).

For anterograde projection mapping experiments, recombinant AAVs expressing GFP and mRuby-fused synaptophysin were unilaterally injected into the parabrachial nucleus of *Pdyn*$^{cre/+}$ mice. After 3–4 weeks, mice were euthanized and processed for histology.

For rabies tracing experiments[39], recombinant AAVs carrying Cre-dependent TVA and G were injected into the parabrachial nucleus of *Pdyn*$^{cre/+}$ mice. After 3 weeks, recombinant EnvA-pseudotyped G-deficient rabies virus (RVΔG) expressing GFP or mCherry was injected into the parabrachial nucleus. RVΔG selectively infects TVA-expressing PB^{Pdyn} neurons, and co-expression of G enables PB^{Pdyn} neurons to complement RVΔG and produce infectious rabies viruses that spread to their direct presynaptic partners. After 8–15 days, mice were euthanized and processed for histology. Five days of expression was insufficient for the complete labelling of the monosynaptic inputs to PB^{Pdyn} neurons. For additional trans-synaptic spread from the monosynaptic inputs to PB^{Pdyn} neurons, a mixture of recombinant AAVs carrying Cre recombinase and Cre-dependent G was injected into the NTS (−7.5 mm AP, ±0.4 mm ML and −5.4 mm DV) or principal sensory trigeminal nucleus (−5.8 mm AP, ±1.4 mm ML and −4.9mm DV) of *Pdyn*$^{cre/+}$ mice at the same time when AAVs carrying Cre-dependent TVA and G were injected into the

parabrachial nucleus. Between 8 and 15 days after RVΔG injection, mice were euthanized and processed for histology.

Gastric and intestinal catheterization and balloon implantation

Intragastric catheters were constructed by penetrating a 6-mm diameter Dacron felt disc with a Silastic tubing (6-cm long, 0.64-mm inner diameter and 1.19-mm outer diameter), fixing at the 2.2-cm position from an end of the tubing using an adhesive (Loctite 401). Mice were anaesthetized with 1.5–3.0% isoflurane, and the surgical areas were shaved and sterilized. A skin incision of about 5 mm in length was made along the dorsal midline, from the base of the skull to the interscapular region. Another skin incision of about 2 cm in length was made along the ventral midline, from the xiphoid cartilage to the left flank, and the subcutaneous tissues were dissected. These two incisions were connected by inserting a sterilized catheter. The stomach was externalized and a small puncture was made using a scissor to insert the catheter, which was sutured into place (NB617, Ailee). The stomach was then placed back in the abdominal cavity, and the abdominal muscle and the skin incision was closed. Lastly, the catheter was secured at the interscapular site with sutures on the skin. For gastric balloon implantation, a latex balloon (7-mm long, 73-3478, Harvard Apparatus) was attached to the end of the intragastric catheter in the stomach using an adhesive (Loctite 401). Following the surgery, mice were provided with liquid food to avoid gastric filling by solid chow. For the duodenum or proximal colon, smaller Silastic tubing (6-cm long, 0.28-mm inner diameter and 0.61-mm outer diameter) was used. Balloon was similarly constructed and implanted in the duodenum or proximal colon.

Vagotomy

Mice were anaesthetized with 1.5–3.0% isoflurane and placed in a stereotaxic apparatus while resting on a heating pad. A midline abdominal incision from the xiphoid process (about 3-cm long) was made along the linea alba to expose the abdominal cavity, and the liver was gently retracted to the left side with cotton swabs. Then, the stomach was moved out of the cavity and kept moisturized with saline throughout the surgery. The oesophagus was gently lifted and all identifiable vagus nerve fibres above the hepatic branches of the anterior vagus (both anterior and posterior vagal trunk) were excised with micro-scissors to achieve total subdiaphragmatic vagotomy. Vagotomy impairs gastric emptying; therefore, all experiments with vagotomized mice were completed within 6 h of the surgery, to avoid any confounding effects caused by the impaired gastrointestinal flow without additional pyloroplasty surgery. Furthermore, mice were provided with liquid food instead of chow food for a day before vagotomy, to minimize the amount of solid ingesta in the stomach during the experiment. To validate total subdiaphragmatic vagotomy, retrograde neural tracer Fluorogold (0.8 mg/0.4 ml in 0.9% saline; sc-358883; Santa Cruz) was intraperitoneally injected into the vagotomized mice or sham surgery control mice. Three days after the injection, mice were euthanized and histologically processed to confirm the absence of Fluorogold in the dorsal motor complex.

Spinal transection

We performed spinal transection at thoracic level (T) 5, corresponding to the highest spinal cord segment at which stomach-innervating splanchnic afferents are joined[40]. Mice were anaesthetized with 1.5–3.0% isoflurane and placed in a stereotaxic apparatus while resting on a heating pad. The surgical areas were shaved and sterilized. A skin incision was made along the dorsal midline at around the T4–T8 level. The incision was expanded with another small incision towards the right flank. Muscles and adipose tissues were cleared from the dorsal spinal lamina. T13 was identified by its dorsal spinous processes, and then T5 was identified by counting eight ribs upwards. The lower spinal cord was gently lifted and thoracic level 5 spinal transection (T5x) was performed using scissors, surgical blades and micro-scissors. Finally, the skin incision was closed. To validate spinal transection, retrograde neural tracer retrobeads (Red RetroBeads; Lumafluor) were injected into the parabrachial nucleus of mice that received T5x or sham surgery control mice. Three days after the injection, mice were euthanized and histologically processed to confirm the absence of retrobeads in the spinal cord.

Fibre photometry

Fibre photometry recordings were performed as previously described[41]. In brief, two excitation lights from 470-nm and 405-nm LEDs (M470F3, M405F1; Thorlabs) were sinusoidally modulated by a real-time processor (RZ5P, Tucker Davis Technologies) at 211 Hz and 531 Hz, respectively, and were collimated and delivered to the brain via a single low-autofluorescence fibre optic patchcord and cannula (400-μm-core, 0.48-NA) (Doric Lenses). The light intensity was maintained at less than 30 μW during all recordings. The fluorescence signal was then focused onto a femtowatt photoreceiver (2151; Newport) for detection, and the resulting signal was demodulated, amplified and collected at around 1 kHz by the RZ5P processor.

To examine the responses of PB^{Pdyn} neurons to water intake, empty-bottle licking and to the intake of various test liquids (except for liquid food), water-deprived mice were placed in a soundproof chamber with lickometers (Med Associates). After 5 min of baseline recording without access to liquid spouts, mice were provided with ad libitum access to the liquids for 20 min. Mice were habituated to the chamber and spouts for at least two days before the tests. Responses of PB^{Pdyn} neurons to liquid food were recorded in food-deprived mice.

To investigate the responses of PB^{Pdyn} neurons to hydrogel, water-deprived mice were provided with ad libitum access for 20 min to hydrogel (consisting of 98% water and 2% of hydrocolloids; ClearH_2O) after 5 min of baseline recording in a behaviour chamber (23 × 43 × 22 cm^3). For chow food or high-fat chow, the same experiments were conducted with food-deprived mice. Mice were acclimated to hydrogel or high-fat chow for at least three days before the tests. The consumption behaviour was recorded using a video camera outside a transparent wall, and the video was analysed frame-by-frame to determine the onset and offset of consumption events. The intake rate of fluids and solids was calculated by dividing total consumed weight by total bout duration.

For the tongue contact experiment, the dorsal surface of the anterior tongue was pressed for 2 s with the round-headed metal tip of the gavage needle (JD-S-124, 0.9 × 70 mm (20G), Jeung Do B&P), with a force of about 51.0 gf. This is in marked contrast with empty-bottle licking (which did not evoke significant responses in PB^{Pdyn} neurons), which is known to exert only approximately 2 gf of force to the anteriormost part of the tongue for around 70 ms[42–44]. For the oesophageal insertion experiments, the gavage needle was slowly inserted into the oesophagus over 3 s, touching and stretching the oesophageal walls, and the needle was stably held for more than 30 s.

To investigate the responses of PB^{Pdyn} neurons to balloon inflation, water or saline was infused into the balloon via catheter using a syringe pump at the indicated rates. At the completion of the experiment, mice were immediately euthanized and the secure connection between the balloon and the catheter was confirmed. Data were discarded if any leakage was detected. For gastric balloon experiments, the balloon was inflated to the volume of 200 μl, 350 μl or 500 μl, which correspond to the less than half of the volume of the unstretched mouse stomach, the volume of the comfortably full mouse stomach or the stretched volume, respectively[45]. For duodenum and colon balloon experiments, the balloon was inflated to 50 μl, which approximately correspond to twice the volume of the intestinal segment occupied by 7-mm-long balloon[46] and to the volume of physiologically distended intestinal segment following the intake of a high-concentration glucose solution[32].

For oral gavage experiments, mice were gently restrained to immobilize the head by a skilled experimenter. A gavage needle attached to

a syringe was brought inside the mouth, or inserted into the pharynx, oesophagus or stomach via the mouth. A small water drop (10 µl), 200 µl of water or oil, or 500 µl of air was injected as indicated. Control experiments (mock) were performed by repeating the same procedure with an empty syringe.

For direct infusion of air into the stomach via intragastric catheter, a syringe pump (GenieTouch, Kent Scientific) was connected to the implanted catheter via a tubing. Air was injected at the indicated rates. For each recording experiment, three trials were averaged and treated as a single replicate.

To examine the responses of PB^{Pdyn} neurons under anaesthesia, mice were anaesthetized with 1.5–3.0% isoflurane. For the oral gavage experiment, 200 µl of water was infused directly into the stomach via oral gavage. For the stomach wall push experiment, a gavage needle was inserted into the digestive tract until it reached the stomach and stably maintained. Then, a sphere-tipped blunt metal probe (approximately 1-mm sphere diameter) was inserted into or withdrawn from the gavage needle, to gently distend the stomach wall while minimizing the mechanical disturbance along the digestive tract. All experiments except for these two were conducted in awake mice.

To examine the responses of PB^{Pdyn} neurons to solutions with different osmolality, taste and temperature, water-deprived mice were head-restrained using a custom-machined metal plate and habituated for >10 min a day for >3 days. The composition of each tastant was as follows: artificial saliva, 4 mM sodium chloride, 10 mM potassium chloride, 6 mM potassium bicarbonate, 6 mM sodium bicarbonate, 0.5 mM calcium chloride, 0.5 mM magnesium chloride, 0.24 mM dipotassium phosphate and 0.24 mM monopotassium phosphate; sweet, 8 mM acesulfame potassium; sour, 10 mM citric acid; salty, 60 mM NaCl; umami, 50 mM monopotassium glutamate and 1 mM inosine monophosphate. Each solution was delivered to the mouth with a 22 gauge metal tube using a pressure injection system operated by transistor–transistor logic (TTL) pulses (GenieTouch, Kent Scientific). The tip of the tube was placed right above the tongue, such that liquid drops formed by the injection directly touched the tongue. For each trial, fluid was injected at a rate of 200 µl/min for 15 s to deliver a total amount of 50 µl. Dotted lines in Extended Data Fig. 2p–r indicate the time at which the operation signal was sent to the syringe pump. The apparent lag in calcium response can largely be explained by the experimental delay of solution delivery to the mouth from the onset of syringe pump action.

For the open field test, mice were placed in an open field arena (50 × 50 cm^2) for 10 min for assessing locomotor activity and anxiety-related features. The centre zone was defined as the 25 × 25 cm^2 square at the centre of the arena. For the elevated plus maze test, mice were placed on an elevated plus maze, consisting of two open and two closed arms (30 × 5 cm^2) extending from a central platform elevated from the ground by 50 cm, for 10 min.

To investigate the responses of PB^{Pdyn} neurons to hypertonic saline injection, euhydrated mice were placed in a behaviour chamber and calcium signals from PB^{Pdyn} neurons were recorded using fibre photometry for 15 min ('pre'). Mice were then intraperitoneally injected with 150 µl of 3 M NaCl, and were recorded for 45 min ('post'). Therefore, a single recording of 60 min was made for each mouse.

To observe the responses of the PB^{Pdyn} neurons to whisker touch, whiskers of gently handled mice were touched by a plastic rod. The side of the whiskers (left or right) was randomly chosen for each trial. A session contained 5 trials with an approximately 30-s inter-trial interval, each of which consisted of 5 whisker stimulations for 5 s. The data collected from left and right whisker stimulations were pooled, as no differences were detected.

To examine the responses of the PB^{Pdyn} neurons to sensory detection of peanut butter, mice were placed in a chamber (18 × 20 × 36 cm^3) with a metal grid floor. After a baseline recording for 5 min, an empty dish was inserted under the grid floor, and then was withdrawn. This was followed by another baseline recording for 5 min, and a small amount of peanut butter placed in another dish was inserted under the floor so that the mice could see and smell, but could not consume, the peanut butter for 5 min.

To test whether PB^{Pdyn} neurons respond to sensory cues paired with water delivery, head-fixed mice received 20 presentations of 10-s tone (3 kHz and 80 dB) that co-terminated with 5-s water delivery into the mouth (inter-trial interval of 60 s). Injected at a rate of 200 µl/min for 5 s, the resulting water drop was about 17 µl in volume. The entire session was repeated daily for four days. To maintain the mice in water-depleted condition for 4 consecutive days, mice were allowed for ad libitum access to water for 2 h daily following the experiment.

To examine the responses of PB^{Pdyn} neurons to water depletion and repletion, euhydrated mice were placed in a behavioural chamber and were recorded for >10 min on day 1 ('BA'). Mice were then returned to home cages and water-deprived for 24 h. On the next day, the dehydrated mice were placed in the behavioural chamber and calcium signals were recorded again for >10 min on day 2 ('WD'). After ad libitum water access for the next 24 h, the euhydrated mice were placed in the behavioural chamber and were recorded again for >10 min ('WR'). Fibre photometry settings were identical for all recording sessions, and all the raw data were normalized by the median fluorescence of day-1 baseline recordings.

To examine the responses of PB^{Pdyn} neurons to systemic CCK injection, CCK dissolved in 0.9% saline (100 µM, 200 µl per mouse) was injected intraperitoneally to the mice during photometry recordings.

All fibre photometry data were analysed with custom-written Matlab (Mathworks) code in combination with the behaviour data collected with Med-PC (Med Associates) or Ethovision (Noldus). The photometry signal was analysed as previously described[41]. Data were low-pass filtered at 2 kHz and downsampled to 100 Hz. A linear function was used to scale the 405-nm channel signal to the 470-nm channel signal to obtain the fitted 405-nm signal. The resulting $\Delta F/F$ was calculated as (raw 470-nm signal − fitted 405-nm signal)/(fitted 405-nm signal) unless otherwise noted. Depending on the experiments, peri-event time plots were created using the TTL timestamps generated by lickometers, timestamps marked by manual frame-by-frame video analysis or timestamps manually marked when infusing fluids directly to the digestive tract. The location of the mouse, the time spent in each chamber and velocity were scored using Ethovision.

Normalized $\Delta F/F$ was calculated by subtracting the average baseline $\Delta F/F$ from individual raw values and by dividing the difference by the baseline standard deviation. For peri-event time plots, the baseline was defined as the 3 s preceding event onset (licking bout, solid contact, passive water delivery to the mouth, tone onset, direct liquid delivery to the digestive tract and so on). The number of licks were counted in 1-s bins to calculate the lick rate shown in peri-event plots.

The bulk responses of PB^{Pdyn} neurons from each mouse to the events were characterized using auROC curve analysis. Receiver–operating characteristic (ROC) curves were calculated by comparing the distribution of $\Delta F/F$ across trials in 100-ms bins, to the distribution of baseline $\Delta F/F$ (3 s before the onset of the events).

In the bar graphs comparing the responses of PB^{Pdyn} neurons to direct fluid injection into the digestive tract via oral gavage or intragastric catheter, $\Delta F/F$ was averaged over a 5-s time window from the infusion onset, unless otherwise noted. A bout for the licking of liquids was defined as any set more than 5 licks, in which no inter-lick interval was greater than 3 s. A bout of solid intake was defined as any continuous action of active consumption. The duration of most bouts of solid intake was longer than 5 s.

To examine the correlation between PB^{Pdyn} neuronal activity and the velocity of mice, data points defined by pairing $\Delta F/F$ with velocity were pooled in 2-cm/s bins for averaging calcium responses and fitted to a linear curve.

Individual variability in the response amplitudes of PB^{Pdyn} neurons within the same experiment is attributable to the exact targeting of

the tip of the fibre optic cannula, as we observed the variability in the response amplitudes even from the same cohort of the mice, which underwent surgery and behavioural experiments on the same dates by the same experimenters using the same protocols. Despite the efforts to collect the data from mice with correct targeting (Extended Data Fig. 2a), the relative positions of the fibre optic cannula tip to the dorsal lateral parabrachial nucleus could still widely vary within the accepted range, which would cause the variability in response amplitudes (as shown in Fig. 2, individual PB^{Pdyn} neurons exhibited varying degrees of response strengths). For example, the intensity of a 532-nm light in the brain tissue could be attenuated to less than 20% of the original intensity after propagating 250 μm (simulated using the Monte Carlo method[47]), which can directly affect the amplitude of the neural responses to behavioural events.

Two-photon calcium imaging

A two-photon microscope (Olympus FVMPE-RS) equipped with a fast resonant scanner, a high-sensitivity, gallium arsenide phosphide photomultiplier tube (PMT) detector, 20× air objective lens with 8.3-mm working distance (Olympus LCPLN20XIR, 0.45 NA), a tunable Mai-Tai laser (Spectra-Physics, Mai-Tai DeepSee) and quadralign 4-axis laser alignment system was used. For all imaging sessions, images were obtained at 5 Hz, using the fast resonant scanner at 30 Hz and a frame averaging of 6. Software was set as the following: laser power, 350–850mW; PMT voltage, 650; gain, 1; offset, 0; scan size, 512 × 512; zoom, 1. For comparing images acquired from different experiments, the same field of view was acquired under the same imaging parameters. For each imaging session, two-photon scanning was triggered by TTL pulses for each trial 30 s before the application of stimuli, and was continuously recorded for the entire session.

Mice were habituated to head fixation and to liquid food, and water-deprived for 1–2 days before imaging under the two-photon microscope. For the intake experiments, 33 μl of water or liquid food was delivered in the mouth at a rate of 200 μl/min for 10 s via a 22-gauge blunt needle using a pressure injection system operated by TTL pulses (GenieTouch, Kent Scientific). Each session consisted of five trials. The experimenter confirmed whether the mice consume the fluid well before and after each session. For the gastric balloon experiments, PBS was injected into, or withdrawn from, the balloon via Silastic tubing at different rates (1.2, 2.1 and 3.5 ml/min for 200, 350 and 500 μl inflation, respectively) for 10 s using the same pressure injection system. Each session consisted of three trials. Balloons remained inflated for 30 s after inflation, and then deflated over the next 10 s. For the oral liquid drop delivery experiments, small drops (less than 10 μl) of water or liquid food were delivered to the mouth as described in 'Fibre photometry', at 600 μl/min for 1 s. The data obtained from the delivery of water and liquid food drops were pooled, as the responses of PB^{Pdyn} neurons were indistinguishable. Each session was consisted of seven trials. Inter-trial intervals were pseudorandomized, with 30-s average intervals for all experiments.

Acquired data were processed by a non-rigid motion correction algorithm (NoRMCorre), and the region of interest for each neuron was defined manually using the standard deviation projection of the movie created by ImageJ. On the basis of the projection images, each neuron was manually registered across different recording sessions. The average fluorescence signals in the region of interest of each neuron were extracted, smoothed with a five-frame running averaging and analysed with a custom-written Matlab code. Normalized F was calculated as normalized $\Delta F/F$ in 'Fibre photometry', except that the baseline was defined as the 5 s before the event onset (that is, passive fluid delivery to the mouth and intragastric balloon inflation). The responses of individual PB^{Pdyn} neurons to the events were characterized using auROC curve analysis. auROC curves were calculated by comparing the distribution of trial-normalized F (0–20 s after the onset of liquid delivery and 0–50 s after the onset of intragastric balloon inflation) to the distribution of baseline F (0–5 s before the onset of the events). Neurons were classified as responsive if the trial-normalized F exceeded 2 s.d. Maximum values for trial-normalized F were used for correlation analysis. A representative water intake session was chosen, and the maximum value for trial-normalized F of each neuron in the session was divided by the maximum value of the highest responding neuron to normalize the activities of all neurons in Fig. 2b.

Optogenetic and chemogenetic manipulations

To stimulate ChR2-expressing neurons or terminals, 5–15 mW of blue light (159–477 mW/mm^2 at the tip of the fibre optic) was generated by a 473-nm laser (MBL-III-473; OEM Laser Systems), and delivered to mice through fibre optic patch cords (0.22 NA, 200-μm diameter; Newdoon). Blue laser output was controlled using a pulse generator (Pulse Pal; Sanworks) to deliver 10-ms light pulse trains at 20 Hz. For chemogenetic experiments, CNO (BML-NS105; Enzo), prepared in 0.9% sterile saline, was injected at 0.3–1 or 10 mg/kg of body weight for hM3Dq or hM4Di experiments, respectively, 45 min before initiation of the behaviour session.

For food intake assays, food-deprived mice were placed in a behaviour chamber (23 × 43 × 22 cm^3) without access to chow food for acclimatization for 10–30 min, and then were provided ad libitum access to chow food for 30 min or 4 h. Food intake was measured by changes in the weight of the food pellet at the indicated time points.

For water intake assays, mice were placed in a soundproof chamber with lickometers (Med Associates). After 5 min of acclimatization, mice were provided with ad libitum access to water for the duration of each session. For 24-h chemogenetic stimulation experiments, mice were provided with ad libitum access to a low-concentration CNO solution (0.0025% (w/v)). Mice were habituated to the chamber and spouts for at least two days before the tests. For optogenetic stimulation experiments, mice were given light pulse trains throughout the 25-min session including acclimatization. For pre-stimulation experiments, mice received laser stimulation for 30 min in a cage and transferred to the chamber with lickometers to begin water intake assays.

For two-bottle tests for assaying water and saline intakes, mice were placed in a soundproof chamber with lickometers (Med Associates). After 5 min of acclimatization, mice were provided with ad libitum access to water and 2% NaCl for 20 min. The liquid bottles were counterbalanced across the left and right sides of the chambers. Mice were habituated to the chamber, spout and liquids for at least two days before the tests. For optogenetic stimulation experiments, mice were given light pulse trains throughout the session including acclimatization. For lick-paired stimulation experiments, 10-ms light pulses were delivered at 20 Hz for 0.1 s upon individual licks. The salt-depleted condition was induced by subjecting mice to intraperitoneal injections of furosemide (a loop diuretic, 10 mg/25 g body weight) and housing them with salt-depleted food and water for 24 h. Water- or food-deprived conditions were induced as described in 'Mice'.

For prandial thirst experiments, food-deprived mice were provided with ad libitum access to the standard chow food in a behavioural chamber without access to water. After 30 min of free-access feeding, mice performed two-bottle tests. Laser stimulation was given throughout the session of each two-bottle test.

For real-time place preference test, mice were placed in a box (50 × 25 × 25 cm^3) consisting of 2 indistinguishable chambers for 15 min. Only one chamber was paired with light stimulation. The choice of paired chamber was counterbalanced across mice. Mice were placed in the unstimulated chamber at the start of the session and received light stimulation initiated upon every entry into the paired chamber.

For social interaction test, a 5-week-old juvenile stranger mouse was introduced into the home cage of a test mouse. After 1-min baseline interaction, a session began with a 'laser on' epoch or a 'laser off' epoch for 1 min. The beginning epochs were counterbalanced, and the epochs were alternated 5 times, such that each session consisted of 10 epochs,

with 5 interleaved laser-on and -off epochs. Social interaction time was measured as the time for which the test mouse actively investigated the intruder. No attack or mounting behaviour was observed in our experiments.

Histology and confocal microscopy

Mice were deeply anaesthetized and were transcardially perfused with ice-cold 4% paraformaldehyde (PFA) in PBS (pH 7.4). Brains or spinal cords were collected, fixed overnight in 4% PFA solution and equilibrated in 30% sucrose in PBS. For collecting spinal segments, the rib cage, diaphragm and organs were removed. T5-L1 segment was identified by counting ribs, then muscle, fat, C1-T4 and L2-S4 spinal segments were isolated. The dorsal surface of the spinal segment was carefully divided in half down the midline. After the tissues reached equilibrium in 30% sucrose PBS solution, 50-µm-thick coronal slices were cut on a freezing microtome. For spinal segment sections, samples were embedded in agarose gel and 100-µm-thick coronal sections were collected. Slices were stored in a cryoprotectant solution (a 5:6:9 mixture of glycerol, ethylene glycol and PBS) at 4 °C until further processed. Free-floating sections were then washed in PBS, incubated for >25 min in 1:10,000–50,000 DAPI solution, washed again in PBS and mounted on microscope slides with PVA-DABCO. Confocal images were obtained on a Zeiss LSM 880 laser scanning microscope using 10×/0.45 NA, 20×/1.0 NA or 40×/1.2 NA objective lens. Images were analysed using IMARIS (Bitplane). For rabies tracing experiments, 300-µm-thick coronal slices were collected, washed in PBS and incubated in 1:5,000 DAPI solution for 24 h. Samples were then incubated in ScaleCUBIC-2 solution (a mixture of 25 wt% urea, 50 wt% sucrose, 10 wt% triethanolamine and 15 wt% distilled water) for 24 h for enhanced transparency[48], followed by mounting with the same solution and imaging.

Abbreviations

The abbreviations used in the figure panels are as follows: 10N, dorsal motor nucleus of the vagus nerve; 12N, hypoglossal nucleus; 3V, third ventricle; 5Tr, trigeminal transition zone; aca, anterior commissure; ad, anterodorsal part of BNST; AMB, nucleus ambiguus; Ap, area postrema; aq, aqueduct; arb, arbor vitae; Arc, arcuate nucleus; BLA, basolateral amygdala; BNST, bed nucleus of the stria terminalis; Cb, cerebellum; CeA, central amygdala; cl, central lateral PB; CO, cochlear nucleus; CU, cuneate nucleus; DB, diagonal band; dl, dorsal lateral PB; DMX, dorsal motor nucleus of the vagus nerve; DR, dorsal raphe nucleus; el, external lateral PB; f, fornix; ic, internal capsule; icp, inferior cerebellar peduncle; IO, inferior olivary complex; LC, locus coeruleus; LH, lateral hypothalamus; lPAG, lateral PAG; LPO, lateral preoptic area; m, medial PB; MCLH, magnocellular nucleus of LH; Me5, mesencephalic trigeminal nucleus; MeA, medial amygdala; mlf, medial longitudinal fascicle; MnPO, median preoptic nucleus; MPA, median preoptic area; NR, nucleus of roller; ns, nigrostriatal tract; NTSim, intermediate NTS; NTSl, lateral NTS; NTSm, medial NTS; NTSpl, posterior-lateral NTS; NTSpm, posterior-medial NTS; opt, optic tract; ov, oval nucleus of BNST; OVLT, vascular organ of lamina terminalis; PAG, periaqueductal grey; PAS, parasolitary nucleus; PB, parabrachial nucleus; PBdl, dorsal lateral PB; PBm, medial PB; PCG, pontine central grey; PLH, posterior LH; Pr5, principal sensory trigeminal nucleus; PRP, nucleus prepositus; PVH, paraventricular hypothalamus; PVT, paraventricular thalamus; RM, nucleus raphe magnus; RN, reticular nucleus; RO, nucleus raphe obscurus; RPA, nucleus raphe pallidus; scp, superior cerebellar peduncle; sctv, ventral spinocerebellar tract; SFO, subfornical organ; SI, substantia innominana; sl, superior lateral PB; SON, supraoptic nucleus; sp5, spinal trigeminal tract; Sp5C, spinal trigeminal nucleus, caudal part; Sp5I, spinal trigeminal nucleus, interpolar part; Sp5O, spinal trigeminal nucleus, oral part; TN, trigeminal nucleus; VII, facial motor nucleus; vl, ventral lateral PB; vlPAG, ventrolateral PAG; VLPO, ventrolateral preoptic nucleus; VN, vestibular nucleus; and VP, ventral pallidum.

Immunohistochemistry

Free-floating 50-µm sections containing the parabrachial nucleus (from −5.0 mm to −5.5 mm AP) obtained as described in 'Histology and confocal microscopy' were washed in PBS and then incubated for 30 min in 0.1% Triton X-100 and 3% normal donkey serum (NDS) (Jackson Immunoresearch) to reduce nonspecific binding. Primary antibody incubation was performed overnight or for 1–2 days at 4 °C in 3% NDS/PBS (rabbit anti-FOS, 1:300–500, 2250S; Cell Signaling Technology; rabbit anti-2A 1:300–500, ABS31; Merck Millipore), followed by washing and incubation with secondary antibodies (Alexa 488- or 647-conjugated donkey anti-rabbit IgG, 1:500, Abcam) for 3 h at room temperature. These sections were washed and stained with DAPI, and mounted as described in 'Histology and confocal microscopy'.

For the water-depletion and repletion experiments, 2 groups of mice expressing fluorophores in PB^{Pdyn} neurons were each single-housed for more than 3 days, water-deprived for 46 h, and water was returned to only 1 group. After 2 h, all mice were perfused and brain sections were prepared.

Fluorescence in situ hybridization

Mice were deeply anaesthetized and were transcardially perfused with ice-cold PBS (pH 7.4). Brains were collected and fresh-frozen on aluminium foil filled with optimal cutting temperature compound (Tissue-Tek) on dry ice. Brains were then stored at −80 °C until further processing. Before sectioning, brains were equilibrated to −21 °C in a cryostat for 60 min. Brains were coronally sectioned at 20 µm and thaw-mounted onto Superfrost Plus slides (25 × 75 × 1 mm^3, Fisherbrand). Brain sections were fixed in 4% PFA for 15 min and then washed in 50%, 70%, 100% and 100% ethanol for 5 min each. Slide-mounted samples were air-dried for 5 min and treated with protease for 30 min. Slides were washed twice in PBS. Probes were previously heated in a 40-°C water bath for 10 min and applied to the slides, which were placed in a 40-°C humidified oven for 2 h. Slides were washed twice in RNAscope wash buffer for 2 min each, and then underwent the amplifier hybridization steps according to the user manual (no. 320293, Advanced Cell Diagnostics). Amplifiers were previously equilibrated at room temperature. After the final hybridization step, samples were counterstained with DAPI (Advanced Cell Diagnostics) for 30 s and coverslips were immediately placed over the tissue section using ProLong Gold Antifade mounting medium (Thermo-Fisher) or Vectashield mounting medium (Vector Labs). We used probes for *Slc32a1* (cat. no. 319191), *Slc17a6* (cat. no. 319171), *Pdyn* (cat. no. 318771), *Fos* (cat. no. 316921), *Oxtr* (cat. no. 412171) and *Calca* (cat. no. 417961).

To validate stimulation of the projection of PB^{Pdyn} neurons to the paraventricular hypothalamus, mice used for the experiment were single-housed for a day. Food and water were removed 30 min before the experiment to prevent confounding effects. Mice were photostimulated for 30 min and immediately killed for the fluorescence in situ hybridization assay for *Fos* expression.

Statistical analysis

Statistical analyses and linear regressions were performed using Matlab (Mathworks) or Prism (GraphPad). We used two-tailed Wilcoxon rank-sum test, Kruskal–Wallis one-way analysis of variance (ANOVA), one-way ANOVA, unbalanced two-way ANOVA with subsequent post hoc correction (Fisher's least significance difference), two-way repeated measures ANOVA with subsequent Bonferroni post-tests, or Pearson correlation, depending on the experimental paradigm. $^{*}P < 0.05$, $^{**}P < 0.01$, $^{***}P < 0.001$, $^{****}P < 0.0001$. Details of the tests and statistical information are shown in Supplementary Table 1. No statistics to determine sample size, blinding or randomization methods were used. Viral expression and implant placement were verified by histology before mice were included in the analysis.

Reporting summary

Further information on research design is available in the Nature Research Reporting Summary linked to this paper.

Data availability

The data that support the findings of this study are available from the corresponding author upon reasonable request.

Code availability

All custom codes are available from the corresponding author upon reasonable request.

35. Kim, E. J., Jacobs, M. W., Ito-Cole, T. & Callaway, E. M. Improved monosynaptic neural circuit tracing using engineered rabies virus glycoproteins. *Cell Rep*. **15**, 692–699 (2016).
36. Miyamichi, K. et al. Dissecting local circuits: parvalbumin interneurons underlie broad feedback control of olfactory bulb output. *Neuron* **80**, 1232–1245 (2013).
37. Guo, Z. V. et al. Procedures for behavioral experiments in head-fixed mice. *PLoS ONE* **9**, e88678 (2014).
38. Namboodiri, V. M. K. et al. Single-cell activity tracking reveals that orbitofrontal neurons acquire and maintain a long-term memory to guide behavioral adaptation. *Nat. Neurosci*. **22**, 1110–1121 (2019).
39. Wickersham, I. R., Finke, S., Conzelmann, K.-K. & Callaway, E. M. Retrograde neuronal tracing with a deletion-mutant rabies virus. *Nat. Methods* **4**, 47–49 (2007).
40. Loukas, M. et al. A review of the thoracic splanchnic nerves and celiac ganglia. *Clin. Anat*. **23**, 512–522 (2010).
41. Lerner, T. N. et al. Intact-brain analyses reveal distinct information carried by SNc dopamine subcircuits. *Cell* **162**, 635–647 (2015).
42. Wang, G. & Fowler, S. C. Effects of haloperidol and clozapine on tongue dynamics during licking in CD-1, BALB/c and C57BL/6 mice. *Psychopharmacology* **147**, 38–45 (1999).
43. Marowitz, L. A. & Halpern, B. P. The effects of environmental constraints upon licking patterns. *Physiol. Behav*. **11**, 259–263 (1973).
44. Rossi, M. A. & Yin, H. H. Elevated dopamine alters consummatory pattern generation and increases behavioral variability during learning. *Front. Integr. Neurosci*. **9**, 37 (2015).
45. McConnell, E. L., Basit, A. W. & Murdan, S. Measurements of rat and mouse gastrointestinal pH, fluid and lymphoid tissue, and implications for *in-vivo* experiments. *J. Pharm. Pharmacol*. **60**, 63–70 (2008).
46. Casteleyn, C., Rekecki, A., Van der Aa, A., Simoens, P. & Van den Broeck, W. Surface area assessment of the murine intestinal tract as a prerequisite for oral dose translation from mouse to man. *Lab. Anim*. **44**, 176–183 (2010).
47. Stujenske, J. M., Spellman, T. & Gordon, J. A. Modeling the spatiotemporal dynamics of light and heat propagation for *in vivo* optogenetics. *Cell Rep*. **12**, 525–534 (2015).
48. Susaki, E. A. et al. Advanced CUBIC protocols for whole-brain and whole-body clearing and imaging. *Nat. Protoc*. **10**, 1709–1727 (2015).
49. Lein, E. S. et al. Genome-wide atlas of gene expression in the adult mouse brain. *Nature* **445**, 168–176 (2007).

Acknowledgements We acknowledge B. K. Lim for the rabies viral vectors; the GENIE Program and the Janelia Farm Research Campus for GCaMP6 materials; T. J. Davidson and K. Deisseroth for help with the fibre photometry setup; H. Lu and U. Oh for help with targeting peripheral ganglia; P. Zhou for help with two-photon image analysis; and Olympus Korea Core Facility of College of Pharmacy of Seoul National University for two-photon microscopy setup. We are grateful to all members of the S.-Y.K. laboratory for helpful discussions, and A. Adhikari, H. Lee, M. E. Carter, J.-W. Sohn and G. S. B. Suh for comments on the manuscript. This work was supported by the National Research Foundation of Korea (NRF) grants funded by the Korean government (MSIP) (no. 2016R1C1B2007319 and no. 2016R1A4A1010796), grants of the Korea Health Technology R&D Project from the Korea Health Industry Development Institute (KHIDI) funded by the Ministry of Health & Welfare, Republic of Korea (grant numbers: HI15C2887 and HI17C2665), Human Frontier Science Program (RGY0064/2017) and Creative-Pioneering Researchers Program of Seoul National University (SNU).

Author contributions D.-Y.K., G.H., M.K. and S.-Y.K. designed the project, interpreted the data and wrote the paper with input from all authors. D.-Y.K., G.H. and M.K. performed all experiments with contributions from H.K., J.A.J., H.-K.K., S.J., M.A., B.H.A., M.L. and G.J.S. H.-E.P. and J.H.P. established the fibre photometry and wrote the code for analysis. J.W.L. contributed to two-photon imaging. S.-Y.K. supervised all aspects of the work.

Competing interests The authors declare no competing interests.

Additional information

Supplementary information is available for this paper at https://doi.org/10.1038/s41586-020-2167-2.

Correspondence and requests for materials should be addressed to S.-Y.K.

Peer review information *Nature* thanks Ivan E. de Araujo, Michael Krashes and Yuki Oka for their contribution to the peer review of this work.

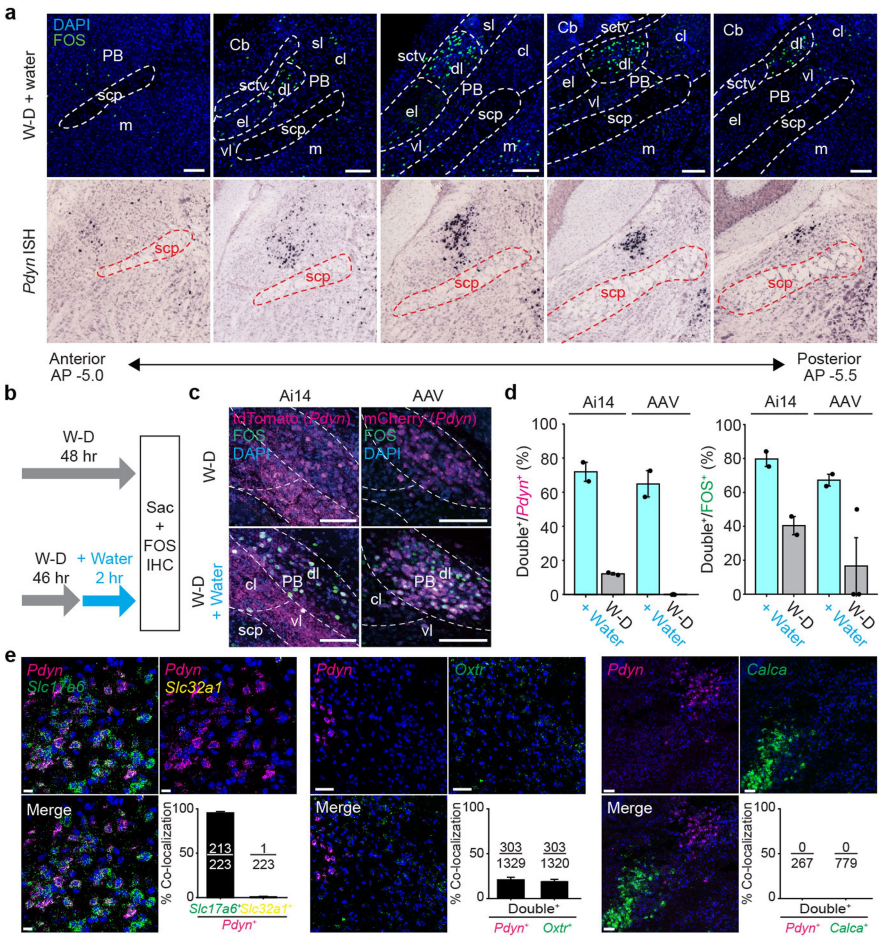

Extended Data Fig. 1 | FOS expression pattern in the parabrachial nucleus following water intake, and overlap of *Pdyn* and other neuronal markers in the parabrachial nucleus. a, We began by probing a marker for neurons of the parabrachial nucleus that signal water intake, as an index of general ingestion. Water intake in dehydrated mice produced robust expression of FOS, a neural activity marker, in the dorsal lateral subnucleus of the parabrachial nucleus (dl), where the gene *Pdyn* (which encodes prodynorphin) is highly expressed. FOS immunofluorescence images (top) and the expression pattern of *Pdyn* from Allen Brain Atlas[49] (bottom) along the AP axis of the parabrachial nucleus. Brain slices were obtained after ad libitum water access following 46-h water restriction. Image credit: Allen Institute. **b**–**d**, To visualize PB^{Pdyn} neurons, we bred a knock-in mouse line expressing Cre recombinase at the *Pdyn* locus (*Pdyn*$^{cre/+}$ mice) with Cre-dependent tdTomato reporter (Ai14) mice. Water-deprived *Pdyn*$^{cre/+}$ Ai14 mice or *Pdyn*$^{cre/+}$ mice injected with a Cre-inducible AAV carrying mCherry were given water access (W-D + water) or not (W-D) before the FOS analysis (**b**). Representative confocal images (**c**) and quantification (**d**) of the overlap between immunolabelled FOS$^+$ and genetically labelled *Pdyn*$^+$ neurons in the PBdl. The majority of tdTomato-expressing *Pdyn*$^+$ neurons were FOS$^+$ (about 72%), whereas few FOS$^+$ neurons were observed in the PBdl of control mice that remained dehydrated (about 12% of *Pdyn*$^+$ neurons). Most FOS$^+$ PBdl neurons were also *Pdyn*$^+$ (about 80%), indicating that *Pdyn* as a useful genetic handle for water-intake-activated neurons in the parabrachial nucleus. We also obtained consistent results in a separate set of experiments using mice in which PB^{Pdyn} neurons were fluorescently labelled using AAV vectors. There were smaller number of FOS$^+$ neurons in the control mice (n = 146 and 7 neurons for experiments using Ai14 mice and AAV vectors, respectively) than in the experimental group (n = 492 and 1,002 neurons for experiments using Ai14 mice and AAV vectors, respectively). **e**, Representative images and quantification of multicolour fluorescence in situ hybridization experiments. *Pdyn*$^+$ neurons are essentially glutamatergic (*Slc17a6*$^+$) (>99%) (left), partially overlapping with fluid-intake-regulating *Oxtr*$^+$ neurons[16] (about 23%) (middle), but are separate from *Calca*$^+$ neurons that have previously been implicated in noxious visceral signalling[18] and meal termination[15] (0%) (right). Scale bars, 100 µm (**a**), 10 µm (**e**), 50 µm (**g**, **i**). Data are presented as mean ± s.e.m. For statistics, see Supplementary Table 1. Abbreviations are defined in 'Abbreviations' in Methods.

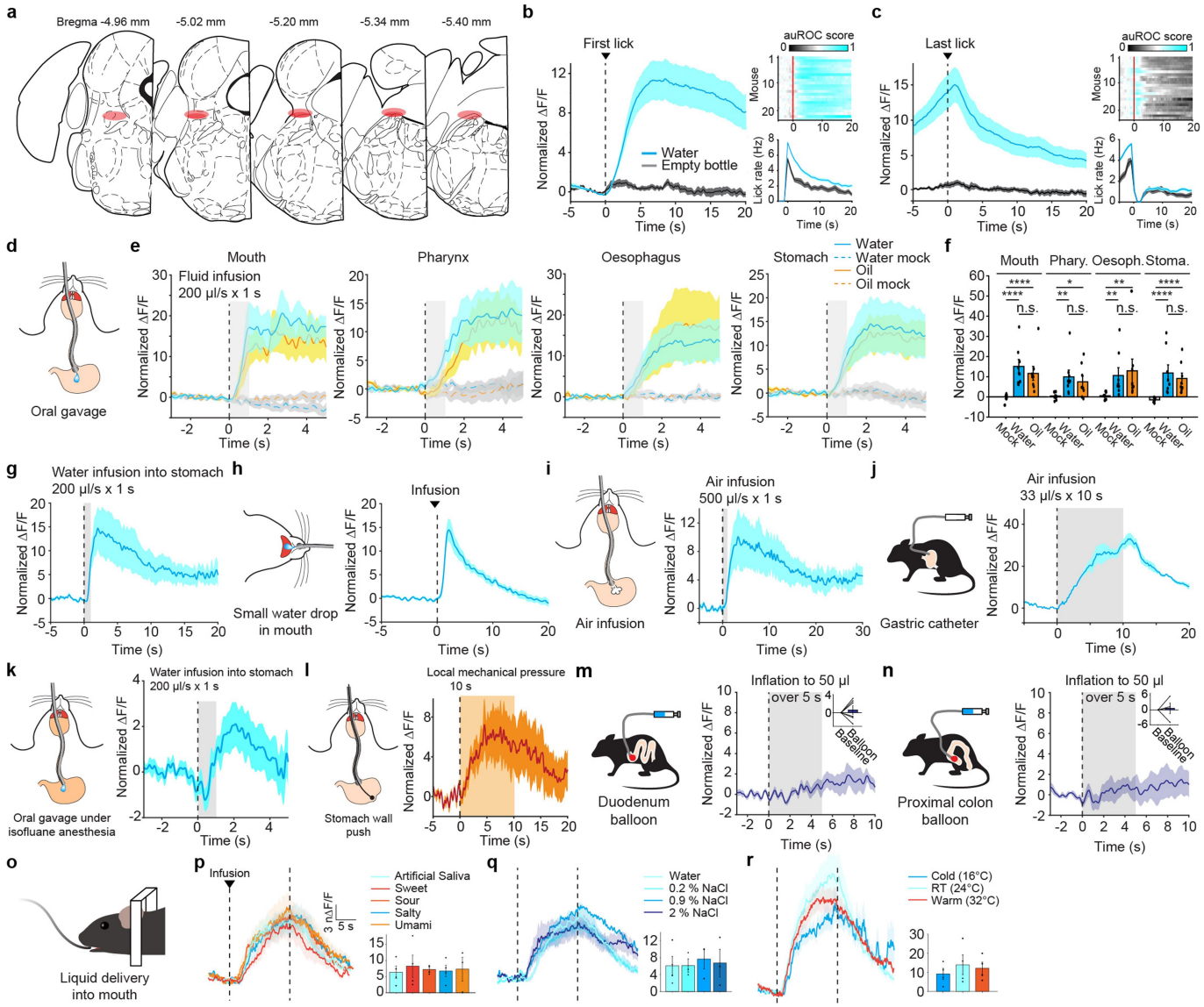

Extended Data Fig. 2 | PB^{Pdyn} neurons monitor ingestion using mechanosensory signals that arise from the upper digestive tract. a, Fibre optic cannula targeting the parabrachial nucleus for fibre photometry were placed inside the red areas. **b**, **c**, Average calcium transients around the first (**b**) or the last lick (**c**) in every bout, showing time-locked responses of PB^{Pdyn} neurons to licking water (blue traces). The act of licking per se is not sufficient to activate PB^{Pdyn} neurons, as there was no response to empty-bottle licking (black). Inset top, average responses of all mice shown as auROC curve heat map. Inset bottom, peri-event plot of lick rate. **d**–**g**, Infusion of water or oil into the mouth, pharynx, oesophagus or stomach via oral gavage (**d**) induced strong activity in PB^{Pdyn} neurons (**e**). Average calcium responses in the first 5 s of infusion (**f**). The rate-controlled infusion of water or silicone oil evoked comparable responses in PB^{Pdyn} neurons, contrary to the uncontrolled voluntary consumption of water and oil (Fig. 1e), consistent with the intake-rate-dependency of the responses (Fig. 1f). Intragastric water infusion with longer intervals reveals the return of the activity to the baseline (**g**). **h**, PB^{Pdyn} neurons robustly responded to oral delivery of a small water drop (10 µl), which would not immediately flow beyond the mouth. **i**,**j**, Intragastric air infusion via oral gavage (**i**) or catheter (**j**) strongly activated PB^{Pdyn} neurons. **k**, Intragastric water infusion via oral gavage in anaesthetized mice also activated PB^{Pdyn} neurons. **l**, Local distension of the stomach wall using a blunt probe in anaesthetized mice robustly activated PB^{Pdyn} neurons. **m**, **n**, PB^{Pdyn} neurons did not significantly respond to the balloon-mediated distension of the duodenum (**m**) or proximal colon (**n**). **o**–**r**, Various test solutions were delivered to the mouth of head-fixed mice (**o**). PB^{Pdyn} neurons exhibited comparable responses to the intake of solutions with different taste (**p**), osmolality (**q**) and temperature (**r**). Insets show average calcium responses in the first 15 s of injection. Dotted lines indicate the onset and offset of infusion. Data are mean ± s.e.m. $^{*}P < 0.05$; $^{**}P < 0.01$, $^{****}P < 0.0001$. n.s., not significant. For statistics, see Supplementary Table 1.

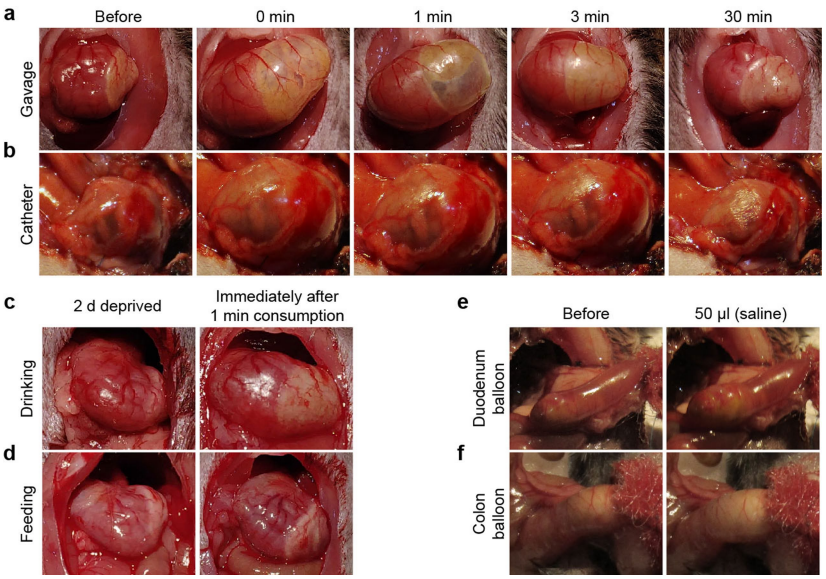

Extended Data Fig. 3 | Gastric and intestinal distension following air infusion, balloon inflation and ingestion. a, b, Representative photographs of the stomach of an anaesthetized mouse before and after intragastric air infusion via oral gavage (**a**) or gastric catheter (**b**). For oral gavage, 1 ml of air was injected over 1 s, and then after 3 s the gavage needle was slowly withdrawn. Mice were rapidly euthanized at the indicated time points, the stomach was exposed and the pictures were taken. For the injection via gastric catheter, 1 ml of air was injected over 10 s. The stomach remained visibly distended at least for 3 min in both cases. **c**, **d**, PB^{Pdyn} neurons respond more strongly to drinking than feeding, as the intake rate is higher for fluids than solids. Although solids are generally considered to distend the stomach more potently than liquids for the slower emptying into the intestine, gastric emptying occurs on the order of tens of minutes, whereas the activity of PB^{Pdyn} neurons evoked by ingestion is on the order of seconds. In accordance with this view, we found that ad libitum intake of water in water-deprived mice for 1 min led to larger distension of the stomach (**c**) than the intake of chow food in food-deprived mice for the same duration (**d**). **e**, **f**, Representative photographs of the balloon-implanted duodenum (**e**) and proximal colon (**f**) before and after the injection of 50 µl saline into the balloon, showing noticeable distension.

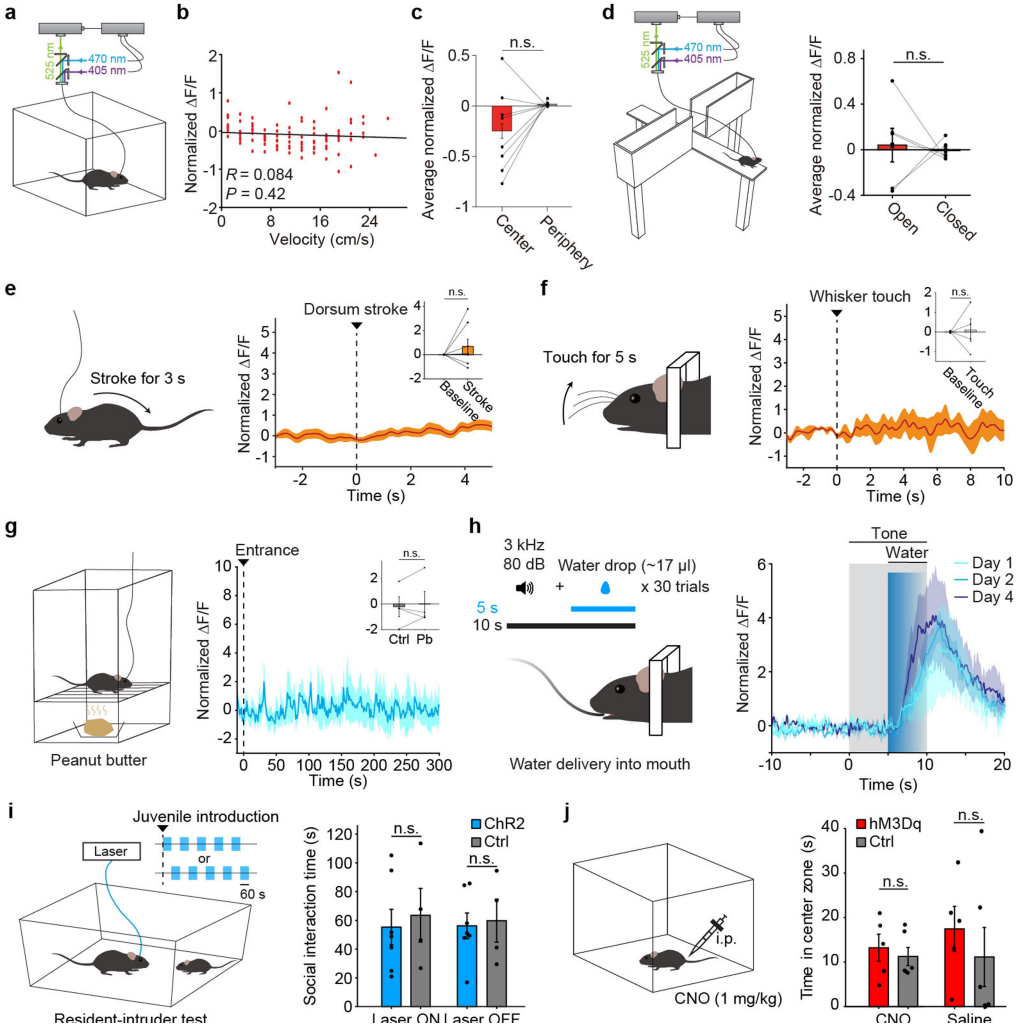

Extended Data Fig. 4 | Control recording and manipulation experiments for PB^{Pdyn}. **a**–**c**, Activity of PB^{Pdyn} neurons was recorded during the open field test (**a**). Activities of PB^{Pdyn} neurons did not correlate with velocity (**b**), and were not significantly different regardless of whether mice were in the centre zone or in the periphery (**c**). **d**, Mice were placed on an elevated plus maze, in which open arms represent an anxiogenic environment. Activities of PB^{Pdyn} neurons were not significantly different regardless of whether mice were in the open or closed arms. **e**, PB^{Pdyn} neurons were not activated by gentle stroking of the dorsum of mice. Peri-event plot of average calcium transients and bar plot of average normalized ΔF/F before and during stroking are shown. **f**, PB^{Pdyn} neurons did not respond to touching of the whisker. **g**, PB^{Pdyn} neurons were not responsive to sensory detection of peanut butter. **h**, Head-fixed, water-deprived mice received 20 tones that co-terminated with water delivery, for 4 days. Average responses of PB^{Pdyn} neurons across training days, showing consistent and robust responses to water delivery (dark blue shaded box) but no responses to the auditory cue (grey shaded box). **i**, Optogenetic stimulation of PB^{Pdyn} neurons did not affect social interaction time with a juvenile stranger mouse. **j**, Chemogenetic stimulation of PB^{Pdyn} neurons did not alter time spent in the centre zone, indicating no change in anxiety-like behaviours. Data are presented as mean ± s.e.m. n.s., not significant. For statistics, see Supplementary Table 1.

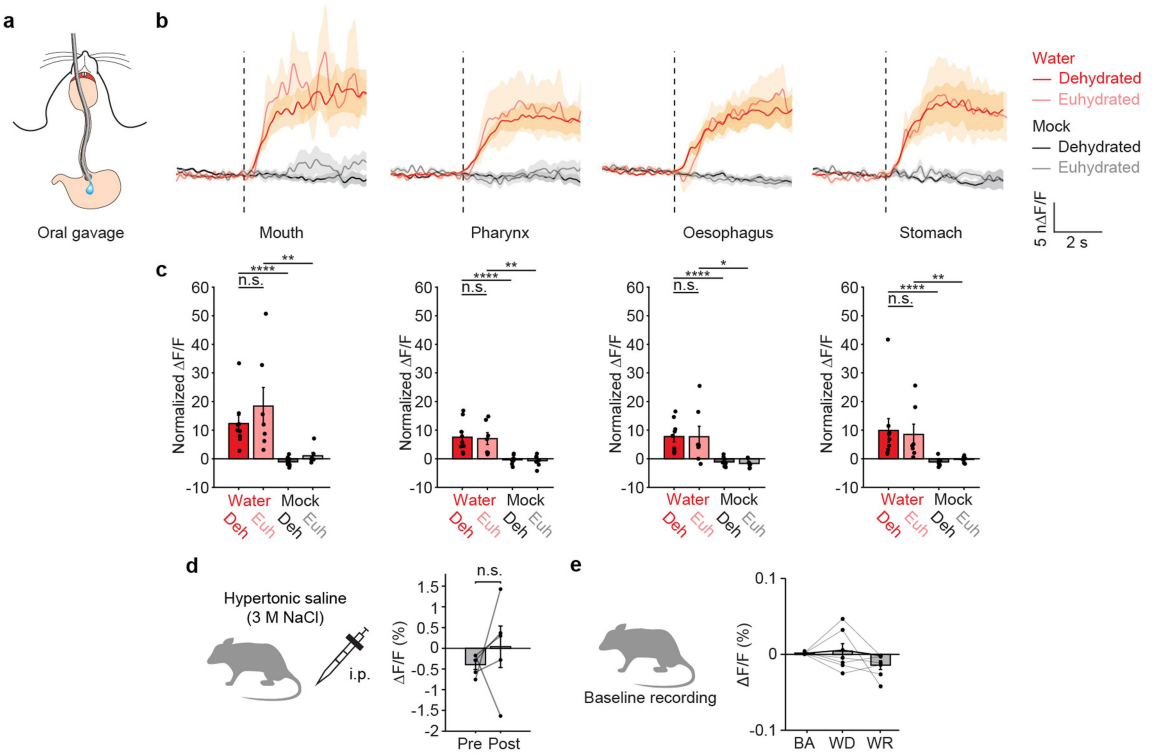

Extended Data Fig. 5 | Activity of PB^{Pdyn} neurons is not modulated by the thirst state. a, Water was directly injected into the mouth, pharynx, oesophagus or stomach of dehydrated or euhydrated mice via oral gavage. **b**, **c**, Peri-event plot of average calcium transients (**b**) and average normalized calcium responses in the first 5 s of injection (**c**). Regardless of whether mice were dehydrated or euhydrated, PB^{Pdyn} neurons were robustly activated by water infused into any part of the upper digestive tract. **d**, **e**, The average calcium activity of PB^{Pdyn} neurons was not different before and after the thirst-inducing hypertonic saline injection (**d**) or 24-h water deprivation (**e**). Data are presented as mean ± s.e.m. $^{*}P < 0.05$; $^{**}P < 0.01$; $^{****}P < 0.0001$. n.s., not significant. For statistics, see Supplementary Table 1.

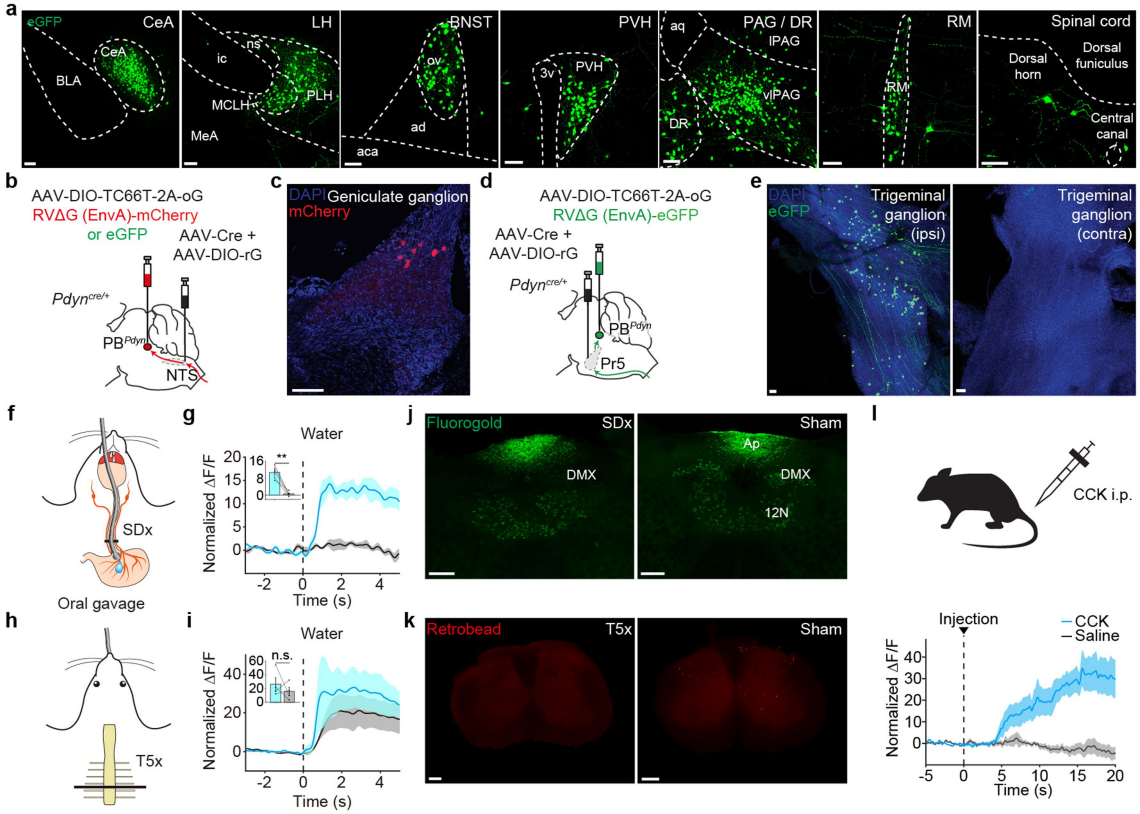

Extended Data Fig. 6 | Mapping inputs to PB^{Pdyn} neurons. a, Identification of monosynaptic inputs to PB^{Pdyn} neurons using engineered rabies virus. Representative confocal images showing the input regions. **b**–**e**, Engineered rabies-virus-mediated identification of monosynaptic inputs to the rostral NTS (**b**) and the Pr5 neurons that project to PB^{Pdyn} neurons (**d**). Representative images showing labelled neurons in the geniculate ganglion projecting to the rostral NTS neurons that project to PB^{Pdyn} neurons (**c**) and neurons in the ipsilateral trigeminal ganglion projecting to the Pr5 neurons that project to PB^{Pdyn} neurons (**e**). **f**–**i**, Total subdiaphragmatic vagotomy (SDx) (**f**) abolished the response of PB^{Pdyn} neurons to intragastric water injection via oral gavage (**g**), but thoracic level 5 spinal transection (T5x) (**h**) did not (**i**). **j**, Validation of subdiaphragmatic vagotomy. Following the intraperitoneal injection of the retrograde neural tracer Fluorogold, many labelled vagal motor neurons were found in the dorsal motor complex (DMX) of the sham control, but not in the vagotomized, mice. **k**, Validation of spinal transection. Following the injection of the retrograde neural tracer Retrobeads (Red RetroBeads; Lumafluor) into the parabrachial nucleus, many labelled neurons were found in the spinal cord of sham control, but not in the spinal-cord-transected, mice. **l**, Both electrophysiological and calcium imaging studies have previously demonstrated that vagal afferents that respond to gastric distension can be activated by CCK, a gut hormone released after a meal[19,22]. If PB^{Pdyn} neurons receive gastric distension signals via mechanosensory vagal fibres, CCK treatment should also activate the PB^{Pdyn} population. Indeed, intraperitoneal CCK injection strongly activated PB^{Pdyn} neurons. Scale bars, 200 μm for (**k**), 100 μm (**a**, **c**, **e**, **j**). Abbreviations are defined in 'Abbreviations' in Methods.

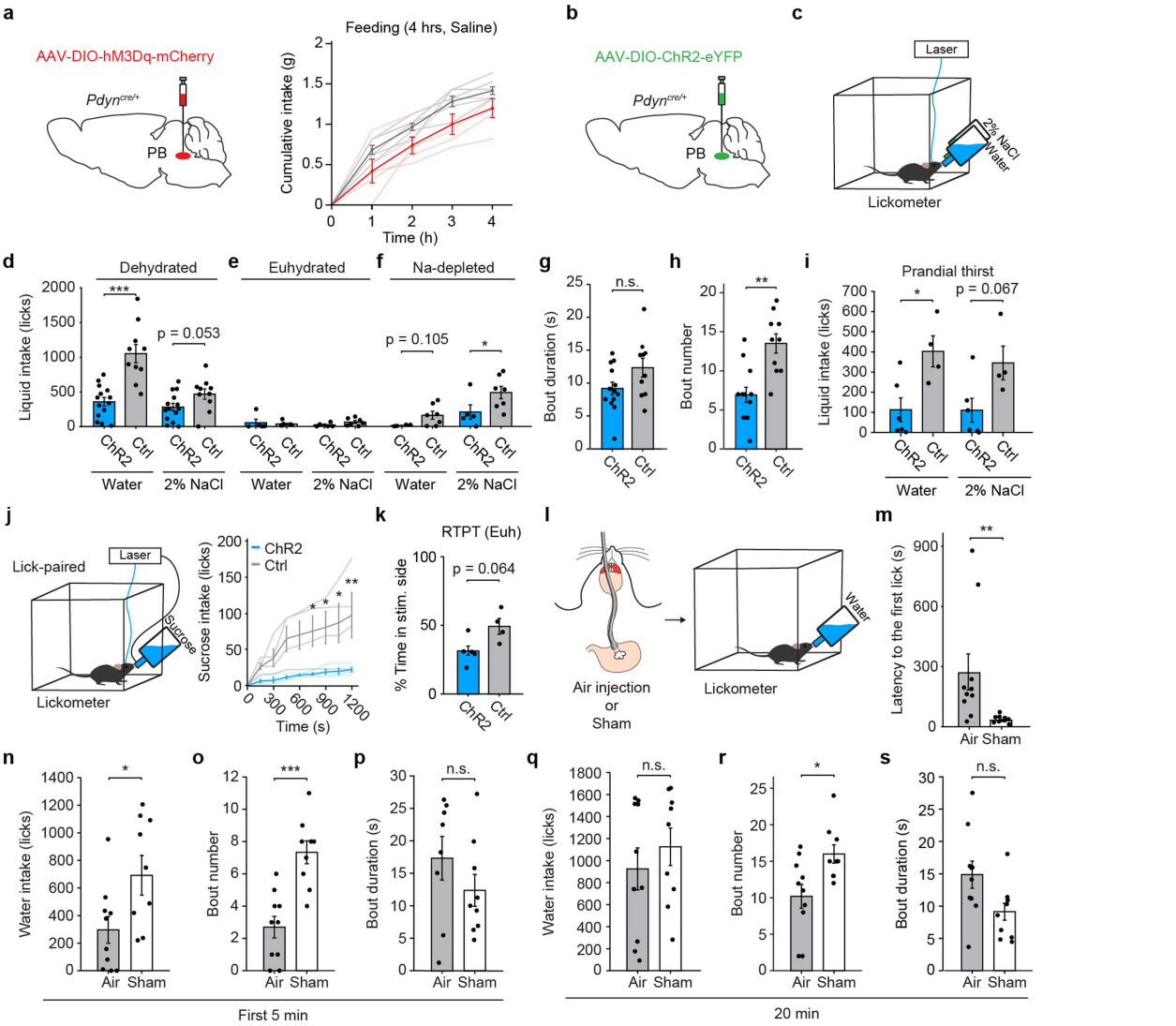

Extended Data Fig. 7 | Activating PB^{Pdyn} neurons suppresses ingestion by reducing bout number rather than bout duration, mimicking the symptoms of gastric distension. a, Saline control experiment for the experiment shown in Fig. 4b. **b**, Optogenetic stimulation of PB^{Pdyn} neurons. **c**, Mice were subjected to a two-bottle test. **d**, In dehydrated mice, optogenetic stimulation of PB^{Pdyn} neurons significantly suppressed water intake and tended to inhibit hypertonic saline intake. **e**, In euhydrated mice, no effect was observed. **f**, In salt-depleted mice, the same manipulation significantly decreased hypertonic saline intake and tended to inhibit water intake. **g**, **h**, The suppression in water intake shown in **d** was not driven by reduced bout duration (**g**) but instead by decreased bout number (**h**). **i**, Food-deprived mice were offered food without water to induce prandial thirst. Stimulating PB^{Pdyn} neurons suppressed water intake and tended to inhibit hypertonic saline intake in mice with prandial thirst. **j**, Ad libitum-fed, euhydrated mice were offered free access to sucrose solution (10%). Lick-paired optogenetic stimulation of PB^{Pdyn} neurons suppressed the intake of sucrose solution. **k**, Optogenetic stimulation of PB^{Pdyn} neurons in euhydrated mice elicited a trend for avoidance in real-time place preference test (RTPT). **l**, Water-deprived mice received intragastric infusion of 1 ml of air (air) or nothing (sham) via oral gavage, and then were provided with free access to water. **m**, Intragastric air infusion significantly increased the latency to the first lick. **n**–**p**, In the first 5 min, The air group consumed significantly smaller amount of water compared with the sham group (**n**). This was driven by decreased bout number (**o**) and not by bout duration (**p**). **q**–**s**, By 20 min from the onset of water intake, the total amount of consumed water became comparable between the two groups (**q**). The air group exhibited a significantly smaller bout number (**r**) and a trend towards longer bout duration (**s**). Data are presented as mean ± s.e.m. $^{*}P < 0.05$, $^{**}P < 0.01$, $^{***}P < 0.001$. n.s., not significant. For statistics, see Supplementary Table 1.

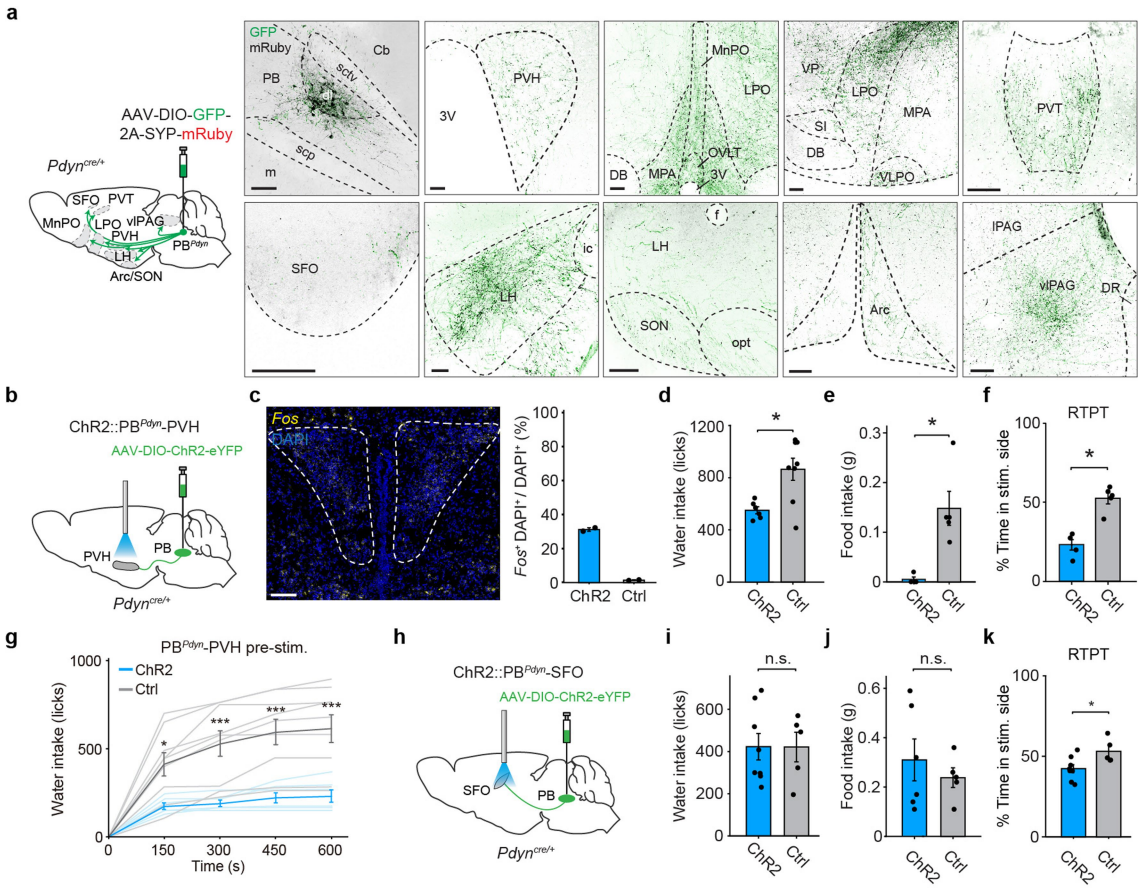

Extended Data Fig. 8 | Projections of PB^{Pdyn} neurons and optogenetic stimulation of the projection to the paraventricular hypothalamus. **a**, Anterograde tracing for visualizing target structures using synaptophysin–mRuby fusion protein. Major PB^{Pdyn}-neuron projection sites are indicated. Representative confocal images showing the parabrachial nucleus injection site and target structures. Green, GFP; black, synaptophysin–mRuby. **b**–**g**, Optogenetic stimulation of PB^{Pdyn} neuron projections to the paraventricular hypothalamus (**b**) activates postsynaptic paraventricular hypothalamus neurons, as indicated by increased *Fos* expression in the paraventricular hypothalamus (**c**). Yellow, *Fos*; blue, DAPI. This manipulation suppressed the intake of both water (**d**) and food (**e**) and induced avoidance in an RTPT (**f**). Pre-stimulation of the PB^{Pdyn} neuron projections to the paraventricular hypothalamus for 30 min before providing access to water elicited sustained inhibition in drinking behaviour in dehydrated mice for at least 10 min (**g**). **h**–**k**, Optogenetic stimulation of PB^{Pdyn} neuron projections to the subfornical organ (**h**) did not affect the intake of water (**i**) or food (**j**), but induced avoidance in an RTPT (**k**). Data are presented as mean ± s.e.m. $^{*}P < 0.05$, $^{***}P < 0.001$, n.s., not significant. For statistics, see Supplementary Table 1. Scale bars, 100 µm. Abbreviations are defined in 'Abbreviations' in Methods.

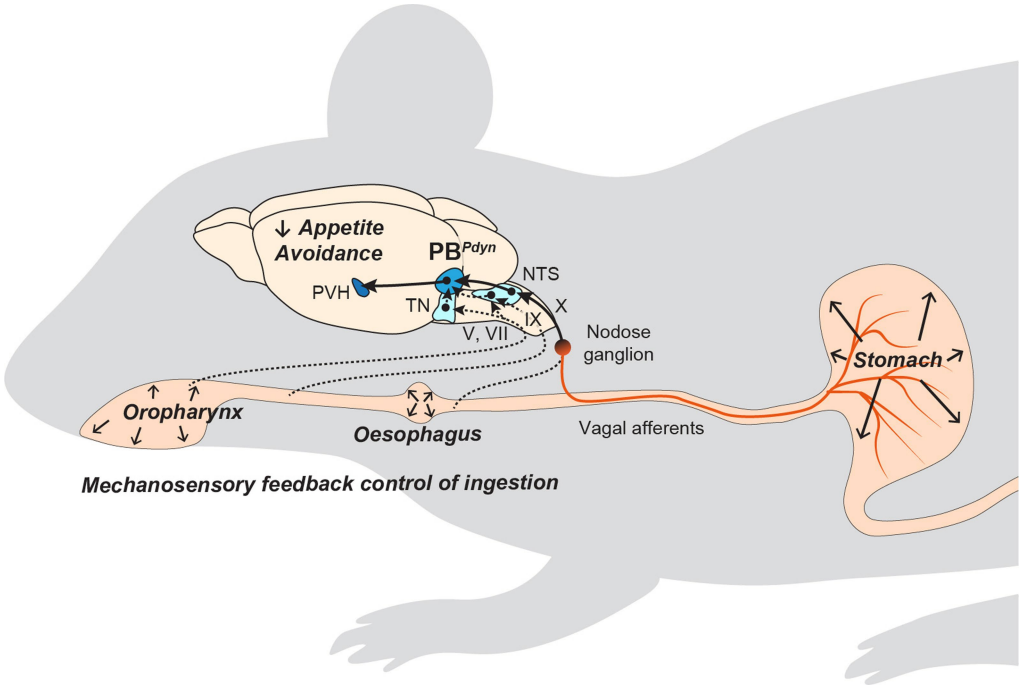

Extended Data Fig. 9 | Summary model. PB^{Pdyn} neurons monitor the intake of both fluids and solids using mechanosensory distension signals from the upper digestive tract, which are transmitted via the cranial nerve pathways (with the vagus nerve conveying the gastric distension signals). The mechanosensory signals from distinct parts along the digestive tract probably converge at the parabrachial nucleus, such that individual PB^{Pdyn} neurons represent integrated mechanosensory signals from all parts of the upper digestive tract. In turn, PB^{Pdyn} neurons transmit sustained appetite-suppressing signals that deter the initiation (but not the maintenance) of ingestive behaviours to the downstream areas (including the paraventricular hypothalamus), to limit excessive feeding and drinking as a negative feedback. Abbreviations are defined in 'Abbreviations' in Methods.

nature research

Corresponding author(s): Sung-Yon Kim

Last updated by author(s): Feb 1, 2020

Reporting Summary

Nature Research wishes to improve the reproducibility of the work that we publish. This form provides structure for consistency and transparency in reporting. For further information on Nature Research policies, see Authors & Referees and the Editorial Policy Checklist.

Statistics

For all statistical analyses, confirm that the following items are present in the figure legend, table legend, main text, or Methods section.

n/a	Confirmed	
☐	☒	The exact sample size (*n*) for each experimental group/condition, given as a discrete number and unit of measurement
☐	☒	A statement on whether measurements were taken from distinct samples or whether the same sample was measured repeatedly
☐	☒	The statistical test(s) used AND whether they are one- or two-sided *Only common tests should be described solely by name; describe more complex techniques in the Methods section.*
☒	☐	A description of all covariates tested
☐	☒	A description of any assumptions or corrections, such as tests of normality and adjustment for multiple comparisons
☐	☒	A full description of the statistical parameters including central tendency (e.g. means) or other basic estimates (e.g. regression coefficient) AND variation (e.g. standard deviation) or associated estimates of uncertainty (e.g. confidence intervals)
☐	☒	For null hypothesis testing, the test statistic (e.g. *F*, *t*, *r*) with confidence intervals, effect sizes, degrees of freedom and *P* value noted *Give P values as exact values whenever suitable.*
☒	☐	For Bayesian analysis, information on the choice of priors and Markov chain Monte Carlo settings
☒	☐	For hierarchical and complex designs, identification of the appropriate level for tests and full reporting of outcomes
☐	☒	Estimates of effect sizes (e.g. Cohen's *d*, Pearson's *r*), indicating how they were calculated

Our web collection on statistics for biologists contains articles on many of the points above.

Software and code

Policy information about availability of computer code

Data collection	TDT Synapse Software (Build 84-33371P), Med-PC IV Software Suite (v4.2), Zeiss ZEN (v2.3), Noldus Ethovision (v11.5), Olympus FV31S-SW (v2.3.2.169)
Data analysis	Graphpad Prism (v7.0, v8.0), MathWorks MATLAB (vR2018b), Bitplane IMARIS (v9.2), ImageJ (v1.52g)

For manuscripts utilizing custom algorithms or software that are central to the research but not yet described in published literature, software must be made available to editors/reviewers. We strongly encourage code deposition in a community repository (e.g. GitHub). See the Nature Research guidelines for submitting code & software for further information.

Data

Policy information about availability of data

All manuscripts must include a data availability statement. This statement should provide the following information, where applicable:

- Accession codes, unique identifiers, or web links for publicly available datasets
- A list of figures that have associated raw data
- A description of any restrictions on data availability

Data and code are available from the corresponding author upon reasonable request.

Field-specific reporting

Please select the one below that is the best fit for your research. If you are not sure, read the appropriate sections before making your selection.

☒ Life sciences ☐ Behavioural & social sciences ☐ Ecological, evolutionary & environmental sciences

Life sciences study design

All studies must disclose on these points even when the disclosure is negative.

Sample size	No statistical methods to pre-determine sample size were used. Sample sizes were based on previous studies in the field of behavioral neuroscience.
Data exclusions	Viral expression of transgenes and implant placement were verified by histology before the data were included in the analysis.
Replication	The key findings of the paper were confirmed by multiple complementary experiments. All behavioral and recording experiments were conducted with sufficient number of animals that exhibited consistent effects. All attempts for replication were successful.
Randomization	Recording experiments entailing multiple trials were randomized whenever possible. For behavioral experiments, mice in each litter were randomly assigned to experimental and control groups before surgery and experiments.
Blinding	Blinding was used to analyze images acquired for in situ hybridization and immunohistochemistry. All other data analyses were automatically performed using MATLAB with the same scripts run for each experimental group.

Reporting for specific materials, systems and methods

We require information from authors about some types of materials, experimental systems and methods used in many studies. Here, indicate whether each material, system or method listed is relevant to your study. If you are not sure if a list item applies to your research, read the appropriate section before selecting a response.

Materials & experimental systems

n/a	Involved in the study
☐	☒ Antibodies
☒	☐ Eukaryotic cell lines
☒	☐ Palaeontology
☐	☒ Animals and other organisms
☒	☐ Human research participants
☒	☐ Clinical data

Methods

n/a	Involved in the study
☒	☐ ChIP-seq
☒	☐ Flow cytometry
☒	☐ MRI-based neuroimaging

Antibodies

Antibodies used

c-Fos (9F6) Rabbit mAb, 1:300-500, 2250S; Cell Signaling Technology
Rabbit anti-2A Peptide Antibody, 1:300-500, ABS31; Merck Millipore
Donkey Anti-Rabbit IgG H&L (Alexa Fluor® 488) preadsorbed, 1:500, ab150061; Abcam
Donkey Anti-Rabbit IgG H&L (Alexa Fluor® 647), 1:500, ab150075; Abcam

Validation

Antibodies were validated by the manufacturers.

c-Fos (9F6) Rabbit mAb: validated by Cell Signaling Technology (https://www.cellsignal.com/products/primary-antibodies/c-fos-9f6-rabbit-mab/2250), tested with the following applications: western blot analysis, immunofluorescent analysis, flow cytometric analysis, and chromatin immunoprecipitation. CiteAb database reports 170 citations for this antibody.

Rabbit anti-2A Peptide Antibody: validated by Merck Millipore (http://www.merckmillipore.com/KR/ko/product/Anti-2A-Peptide-Antibody,MM_NF-ABS31?bd=1#documentation), tested with the western blot analysis. CiteAb database reports 27 citations for this antibody.

Donkey Anti-Rabbit IgG H&L (Alexa Fluor® 488) preabsorbed: validated by Abcam (https://www.abcam.com/donkey-rabbit-igg-hl-alexa-fluor-488-preadsorbed-ab150061.html), tested with the following applications: Immunofluorescence, Immunocytochemistry/Immunofluorescence, Flow Cytometry, ELISA, and Immunohistochemistry (both PFA-fixed paraffin-embedded sections and frozen sections). CiteAb database reports 23 citations for this antibody.

Donkey Anti-Rabbit IgG H&L (Alexa Fluor® 647): validated by Abcam (https://www.abcam.com/donkey-rabbit-igg-hl-alexa-fluor-647-ab150075.html), tested with the following applications: Immunocytochemistry/Immunofluorescence, Flow Cytometry, ELISA, and Immunohistochemistry (both PFA-fixed paraffin-embedded sections and frozen sections). CiteAb database reports 83 citations for this antibody.

Animals and other organisms

Policy information about studies involving animals; ARRIVE guidelines recommended for reporting animal research

Laboratory animals	Both male and female mice at least six weeks of age were used for data collection. C57BL/6J (JAX stock no. 000664), PdynCre/+ (JAX stock no. 027958) and Gt(ROSA)26Sortm14(CAG-tdTomato)Hze/J (Ai14 mice; JAX stock no. 007914) mice were obtained from the Jackson Laboratory. All mice used for experiments were heterozygotes maintained on the C57BL/6J background.
Wild animals	No wild animals were used.
Field-collected samples	No field-collected samples were used.
Ethics oversight	Experimental procedures were performed in compliance with the Guide for the Care and Use of Laboratory Animals from the Seoul National University, and approved by the Seoul National University Institutional Animal Care and Use Committee.

Note that full information on the approval of the study protocol must also be provided in the manuscript.